

Perfectly Balanced: Improving Transfer and Robustness of Supervised Contrastive Learning

Mayee F. Chen^{*1}, Daniel Y. Fu^{*1}, Avanika Narayan¹, Michael Zhang¹, Zhao Song², Kayvon Fatahalian¹, and Christopher Ré¹

¹Department of Computer Science, Stanford University

²Adobe Research

¹{mfchen, danfu, avanikan, mzhang, kayvonf, chrismre}@cs.stanford.edu

²zsong@adobe.com

Abstract

An ideal learned representation should display transferability and robustness. Supervised contrastive learning (SupCon) is a promising method for training accurate models, but produces representations that do not capture these properties due to class collapse—when all points in a class map to the same representation. Recent work suggests that “spreading out” these representations improves them, but the precise mechanism is poorly understood. We argue that creating spread alone is insufficient for better representations, since spread is invariant to permutations within classes. Instead, both the correct degree of spread and a mechanism for breaking this invariance are necessary. We first prove that adding a weighted class-conditional InfoNCE loss to SupCon controls the degree of spread. Next, we study three mechanisms to break permutation invariance: using a constrained encoder, adding a class-conditional autoencoder, and using data augmentation. We show that the latter two encourage clustering of latent subclasses under more realistic conditions than the former. Using these insights, we show that adding a properly-weighted class-conditional InfoNCE loss and a class-conditional autoencoder to SupCon achieves 11.1 points of lift on coarse-to-fine transfer across 5 standard datasets and 4.7 points on worst-group robustness on 3 datasets, setting state-of-the-art on CelebA by 11.5 points.

1 Introduction

Learning a representation with a favorable geometry is a critical challenge for modern machine learning. Good geometries can engender strong downstream transfer performance and robustness to subgroup imbalances, whereas poor geometries may have low transferability and be brittle [25, 37]. However, producing—or even characterizing—a good geometry can be difficult.

We focus on the challenges in doing so with supervised contrastive learning (SupCon). SupCon is a promising method for training accurate machine learning models [27], but suffers from class collapse—wherein each point in the same class has the same representation, as in Figure 1 far left [19]. Collapsed representations cannot distinguish fine-grained details within classes—in particular *latent subclasses*—resulting in poor transferability and robustness. Modifications to SupCon that heuristically “spread out” its representations have shown empirical promise [25], but a precise understanding of spread—how separated individual points are in representation space—and how to control it is lacking.

Furthermore, spread alone is not sufficient to explain improved representations. We observe that modifications to SupCon that increase spread are invariant to *class-fixing permutations*. That is, the loss value does not change when points of the same class are arbitrarily permuted in representation space. For example, Figure 1 right visualizes two geometries that both have spread but differ in representation quality, as suggested by the significant gap in transfer

^{*}Equal Contribution.

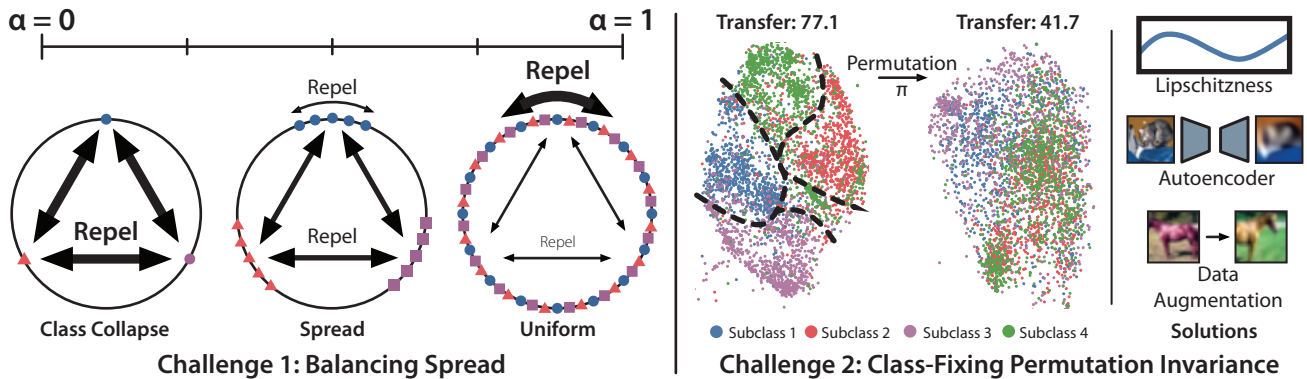


Figure 1: There are two key challenges to achieving better representations with SupCon. Left: The first challenge is balancing multiple contrastive loss terms with competing geometries. We show that adding a weighted class-conditional InfoNCE term can balance the geometries and induce spread in the representation geometry. Right: The second challenge is that representation geometries are invariant to class-fixing permutations. The two example geometries shown both have spread, but vastly different coarse-to-fine transfer performance. We analyze three mechanisms for addressing this challenge: constraining the encoder, adding a class-conditional autoencoder, and using data augmentation. Best viewed in color.

learning performance (35.4 points). Thus, while spread may be important, another mechanism is needed to break class-fixing permutation invariance for good performance.

We argue that these are the two key challenges to improving SupCon’s representations: creating the correct degree of spread, and breaking class-fixing permutation invariance. This paper makes progress on these challenges.

Challenge 1: Balancing Spread. We first prove a simple result that a class-collapsed representation cannot have good transfer performance, which motivates spread. We then analyze whether L_{spread} , a loss function that combines SupCon with a class-conditional InfoNCE loss, can induce spread.

We find that previous approaches for analyzing contrastive losses encounter a technical challenge because SupCon and InfoNCE have incompatible optimal geometries (class collapse and uniformity on the hypersphere, respectively). For example, Wang and Isola [42] analyze individual loss components in isolation, but doing so risks drawing misleading conclusions when the loss components are incompatible. Further, finding exact solutions to optimization problems on the hypersphere is fundamentally difficult; a classic example is the Thomson problem [38], which has evaded an exact solution after a century of study.

We bypass these problems by constructing a distribution that is neither collapsed nor uniform and analyzing its loss. We introduce $s_f(y)$, a notion of class variance, to measure spread on this distribution, and show that it has an intermediate degree of spread. We derive bounds for a weight α on the class-conditional InfoNCE loss within which this distribution attains lower loss than either extreme. While this result does not fully characterize the geometry, it suggests that setting α properly can induce an optimal distribution with appropriate spread—which we validate with measurements on CIFAR10.

Challenge 2: Breaking Permutation Invariance. Our first result demonstrates that L_{spread} can induce spread but does not give insight on class-fixing permutation invariance. We define class-fixing permutation invariance and prove that L_{spread} is subject to it absent other interventions.

This motivates the question: how should we break class-fixing permutation invariance? We show that inducing an inductive bias towards clustering of latent subclasses can break permutation invariance—and more importantly, can result in good coarse-to-fine transfer performance. We introduce $\sigma_f(z)$, a measure of subclass clustering, and show that coarse-to-fine generalization error scales with $\sigma_f(z)/s_f(y)$.

A standard approach to bounding $\sigma_f(z)$ is assuming Lipschitzness. However, Lipschitzness is a strong assumption for modern deep networks, which are powerful enough to memorize random noise [44]. In empirical measurements, we find that modern deep networks display poor Lipschitzness, and thus the Lipschitzness assumption is insufficient for inducing clustered subclass representations.

We thus propose two alternatives that can control $\sigma_f(z)$ under more realistic assumptions: directly encoding fine-

grained details by concatenating the representations from a class-conditional autoencoder, and using data augmentation in the class-conditional InfoNCE loss. The former only requires a “reverse Lipschitz” decoder to upper bound $\sigma_f(z)$, and can do so by a constant factor tighter than a general (non-conditional) autoencoder. The latter only requires the encoder to be Lipschitz over data augmentations to induce subclass clustering—and can also explain observations from prior work [25]. We validate these findings by measuring Lipschitzness constants and $\sigma_f(z)/s_f(y)$ on real data; we find that the assumptions required are more realistic than overall Lipschitzness, and that data augmentation and autoencoders help induce subclass clustering.

Empirical Validation Using our theoretical insights, we propose THANOS: adding a class-conditional InfoNCE loss and a class-conditional autoencoder to SupCon. We evaluate THANOS on two tasks designed to evaluate how well it preserves subclasses:

- **Coarse-to-fine transfer learning** trains a model to classify superclasses but use the representations to distinguish subclasses. THANOS outperforms SupCon by 11.1 points on average across 5 standard datasets.
- **Worst-group robustness** evaluates how well a model can identify underperforming sub-groups and maintain high performance on them. THANOS identifies underperforming sub-groups 7.7 points better than previous work [37] and achieves 4.7 points of lift on worst-group robustness across 3 datasets, setting state-of-the-art on CelebA by 11.5 points. THANOS can even outperform GroupDRO [36], a state-of-the-art robustness algorithm that uses *ground-truth* sub-group labels.

2 Background

Section 2.1 presents our data model and the coarse-to-fine transfer task. Section 2.2 presents L_{spread} , a simple variant of SupCon that adds a weighted class-conditional InfoNCE loss. Section 2.3 discusses geometry of contrastive losses.

2.1 Data Setup

Input data $x \in \mathcal{X}$ are drawn from a distribution \mathcal{P} with deterministic class $y = h(x)$, where $y \in \mathcal{Y} = \{0, \dots, K-1\}$. We assume that the data is class-balanced such that $\Pr(y = i) = \frac{1}{K}$ for all $i \in \mathcal{Y}$.

Data points also belong to *latent subclasses*. Following Sohoni et al. [37], we denote a subclass as a latent discrete variable $z \in \mathcal{Z}$. \mathcal{Z} can be partitioned into disjoint subsets S_0, \dots, S_{K-1} such that if $z \in S_k$, then its corresponding y label is equal to k . For simplicity, we assume that there are two subclasses for each label k , e.g. $|S_k| = 2$. The data generating process proceeds as follows: first, the latent subclass z is sampled with proportion $p(z)$. Then, x is sampled from the distribution $\mathcal{P}_z = p(\cdot|z)$, and its corresponding deterministic label is denoted $y = S(z)$. Let $h_s(x) : \mathcal{X} \rightarrow \mathcal{Z}$ denote x ’s subclass.

We have a class-balanced labeled training dataset $\mathcal{D} = \{(x_i, y_i)\}_{i=1}^n$ where points (x_i, z_i, y_i) are drawn i.i.d, and the value of each z_i is unknown during training time. Denote $\mathcal{D}_y = \{x \in \mathcal{D} : h(x) = y\}$ and $\mathcal{D}_z = \{x \in \mathcal{D} : h_s(x) = z\}$, and denote their sizes by $n_y = |\mathcal{D}_y|$ and $n_z = |\mathcal{D}_z|$.

Contrastive learning involves training an encoder $f : \mathcal{X} \rightarrow \mathbb{R}^d$ on \mathcal{D} that maps inputs to representations in an embedding space \mathbb{R}^d .

Coarse-to-Fine Transfer Coarse-to-fine transfer evaluates how well an embedding trained on the coarse classes \mathcal{Y} distinguishes fine classes (subclasses) z . Suppose that $S_y = \{z, z'\}$. The coarse-to-fine transfer task aims to classify z versus z' using the encoder f learned on \mathcal{D} . We are given a dataset of subclass labels, $\mathcal{D}_s = \{(x_i, z_i)\}_{i=1}^m$. Denote $\mathcal{D}_{s,z} = \{x \in \mathcal{D}_s : h_s(x) = z\}$ and $m_z = |\mathcal{D}_{s,z}|$. We learn linear weights $W_z, W_{z'} \in \mathbb{R}^d$ and construct an estimate $\hat{p}(z|f(x))$ by using softmax scores $\hat{p}(z|f(x)) = \frac{\exp(f(x)^\top W_{h_s(x)})}{\exp(f(x)^\top W_z) + \exp(f(x)^\top W_{z'})}$, where f is fixed. We use the mean classifier to construct W , following prior work [2]. That is, $W_z = \frac{1}{m_z} \sum_{x \in \mathcal{D}_{s,z}} f(x)$, and $W_{z'}$ is similarly defined.

We evaluate the performance of coarse-to-fine transfer with a γ -margin loss, defined on a point (x, z) as

$$\ell_{\gamma, f}(x, z) = 1 - \mathbb{1} \{ \hat{p}(z|f(x)) \geq \gamma \hat{p}(z'|f(x)) \} \quad (1)$$

for $\gamma > 1$. That is, we want the model to output the correct subclass label at least γ times more likely than the incorrect one. Define the γ -margin generalization error on z as $L_{\gamma,f}(z) = \mathbb{E}_{x \sim \mathcal{P}_z} [\ell_{\gamma,f}(x, z)]$.

2.2 A Modified Supervised Contrastive Loss

Contrastive learning trains an encoder to produce representations of the data by pushing together similar points (positive pairs) and pulling apart different points (negative pairs). We consider L_{spread} , a weighted sum of a supervised contrastive loss L_{sup} [27] and a class-conditional InfoNCE loss L_{cNCE} .

Let B be a batch of data from \mathcal{D} . Define $P(i, B) = \{x^+ \in B \mid i : h(x^+) = h(x_i)\}$ as the points with the same label as x_i and $N(i, B) = \{x^- \in B \mid i : h(x^-) \neq h(x_i)\}$ as points with a different label. Let $a(x_i)$ be an augmentation of x_i , and we assume that augmentations of each sample are disjoint. Denote $\sigma_f(x, x') = \exp(f(x)^\top f(x') / \tau)$ with temperature hyperparameter τ . For $\alpha \in [0, 1]$, $L_{\text{spread}}(f, x, B)$ on x belonging to B is:

$$L_{\text{spread}}(f, x, B) = (1 - \alpha)L_{\text{sup}}(f, x, B) + \alpha L_{\text{cNCE}}(f, x, B),$$

where

$$L_{\text{sup}}(f, x_i, B) = -\frac{1}{|P(i, B)|} \sum_{x^+ \in P(i, B)} \log \frac{\sigma_f(x_i, x^+)}{\sigma_f(x_i, x^+) + \sum_{x^- \in N(i, B)} \sigma_f(x_i, x^-)}, \quad (2)$$

$$L_{\text{cNCE}}(f, x_i, B) = -\log \frac{\sigma_f(x_i, a(x_i))}{\sum_{x^+ \in P(i, B)} \sigma_f(x_i, x^+)}. \quad (3)$$

The overall loss $L_{\text{spread}}(f, B)$ is averaged over all points in B . L_{sup} is a variant of the SupCon [27] loss. L_{cNCE} is a class-conditional version of the InfoNCE loss, where the positive distribution consists of augmentations and the negative distribution consists points from the same class, intuitively encouraging them to be spread apart.

2.3 Geometries of Contrastive Losses

We present a series of standard theoretical assumptions for analyzing contrastive geometry, and define two important distributions—class collapse and class uniformity.

Assumptions We make several standard theoretical assumptions [19, 42, 35]: 1) restrict the encoder f 's output space to be \mathcal{S}^{d-1} , the unit hypersphere (i.e. normalized outputs); 2) assume that $K \leq d + 1$, such that a K -regular simplex inscribed in \mathcal{S}^{d-1} exists; 3) assume that the encoder is *infinitely powerful*, meaning that any distribution on \mathcal{S}^{d-1} is realizable by $f(x)$. We define the pushforward measure of the class-conditional distribution of $p(\cdot \mid h(x) = y)$ via f as μ_y for $y \in \mathcal{Y}$, where $\mu_y \in \mathcal{M}(\mathcal{S}^{d-1})$ is over all Borel probability measures on the hypersphere. Define $\mu = \{\mu_y\}_{y \in \mathcal{Y}}$ as the overall pushforward measure corresponding to $\mathcal{P} \circ f^{-1} \in \mathcal{M}(\mathcal{S}^{d-1})$.

Class Collapse Distribution Define $\mathbf{v} = \{v_y\}_{y \in \mathcal{Y}} \in \mathcal{S}^{d-1}$ as the set of vectors forming the regular simplex inscribed in the hypersphere, satisfying: a) $1^\top \mathbf{v} = 0$; b) $\|v_y\|_2 = 1 \forall y$; and c) $\exists c_K \in \mathbb{R}$ s.t. $v_y^\top v_{y'} = c_K$ for $y \neq y'$. Let δ_{v_y} be the probability measure on \mathcal{S}^{d-1} with all mass on v_y , and let $\delta_{\mathbf{v}} = \{\delta_{v_y}\}_{y \in \mathcal{Y}}$ be the *class-collapsed measure* such that $f(x) = v_y$ almost surely whenever $h(x) = y$. Graf et al. [19] show that $\mu = \delta_{\mathbf{v}}$ minimizes the SupCon loss.

Class Uniform Distribution Denote σ_{d-1} as the normalized surface area measure on \mathcal{S}^{d-1} . $\mu = \sigma_{d-1}$ is the *class-uniform measure* when $\mu_y = \sigma_{d-1}$ for all $y \in \mathcal{Y}$. Wang and Isola [42] show that σ_{d-1} minimizes the InfoNCE loss.

3 Controlling Spread

In Section 3.1, we demonstrate the importance of spread—having distinguishable representations of points in a class—by showing that SupCon results in poor coarse-to-fine transfer. In Section 3.2, we begin to explore whether L_{spread} can result in more spread out geometries. We introduce an asymptotic form of L_{spread} and apply the approach from Wang and Isola [42] to analyze individual loss terms. We find that the optimal geometries of the individual

terms are incompatible. In Section 3.3, we analyze the asymptotic L_{spread} as a whole using a nuanced approach that compares the loss over different geometries. We conclude that the optimal geometry is neither class-collapsed nor class-uniform for a range of α . This result suggests that spread can be carefully controlled, and we capture this property by introducing a notion of intra-class variance, $s_f(y)$. All proofs for the paper are in Appendix C.

3.1 The Importance of Spread

SupCon exhibits class collapse and does not spread out representations in a class. We show that this geometry results in poor coarse-to-fine generalization error: asymptotically, the error obtains its maximum possible value.

Define $f_{SC} \in \mathcal{F}$ to be the encoder trained with SupCon satisfying $f_{SC}(x) = v_y$ for all $x \in \mathcal{D}$ where $h(x) = y$. Let $f(x)[j]$ be the j th entry of $f(x)$. For function class \mathcal{F} , let $\mathcal{F}_j = \{f(\cdot)[j] : f \in \mathcal{F}\}$ be the elementwise class. Let $\mathfrak{R}_n(\mathcal{F}_j)$ denote \mathcal{F}_j 's Rademacher complexity on n samples, and define $\mathfrak{R}_n(\mathcal{F}) = \sum_{j=1}^d \mathfrak{R}_n(\mathcal{F}_j)$.

Theorem 1. For γ where $\log \gamma \geq 8 \max\{\mathfrak{R}_{n_z}(\mathcal{F}), \mathfrak{R}_{n_{z'}}(\mathcal{F})\}$, SupCon's coarse-to-fine error is at least

$$L_{\gamma, f_{SC}}(z) \geq 1 - \delta(n_z, \mathcal{F}, \gamma) - \delta(n_{z'}, \mathcal{F}, \gamma) - \xi(m_z \wedge m_{z'}, \gamma),$$

where $\delta(n_z, \mathcal{F}, \gamma) = d \exp\left(-\frac{n_z}{32d^2}(\log \gamma - 8\mathfrak{R}_{n_z}(\mathcal{F}))^2\right)$ bounds generalization error of f_{SC} and $\xi(m_z \wedge m_{z'}, \gamma) = 4d \exp\left(-\frac{(m_z \wedge m_{z'}) \log^2 \gamma}{32d}\right)$ bounds the noise from \mathcal{D}_s .

As $n \wedge m$ increases, error approaches 1—its maximum value—and the model will almost surely predict the correct subclass γ times less often than the incorrect one. This result motivates an analysis of whether L_{spread} can encourage spread.

3.2 Asymptotic L_{spread}

We present an asymptotic version of L_{spread} . For a given anchor $x \sim \mathcal{P}$, define a positive pair $x^+ \sim p(\cdot | h(x^+) = h(x))$ from the same class and a negative pair using $x^- \sim p(\cdot | h(x^-) \neq h(x))$ from a different class. Let $a(x)$ be an augmentation of x drawn from a distribution $p_a(\cdot | x)$, where each $p_a(\cdot | x)$ has disjoint support.

Definition 1. Define $L_{\text{spread}}(f, \alpha)$ as

$$L_{\text{spread}}(f, \alpha) = (1 - \alpha)L_{\text{align}}(f) + \alpha L_{\text{aug}}(f) + (1 - \alpha)L_{\text{diff}}(f) + \alpha L_{\text{same}}(f),$$

where

$$\begin{aligned} L_{\text{align}}(f) &= \mathbb{E}_{x, x^+} [\|f(x) - f(x^+)\|^2 / 2\tau] \\ L_{\text{aug}}(f) &= \mathbb{E}_{x, a(x)} [\|f(x) - f(a(x))\|^2 / 2\tau] \\ L_{\text{diff}}(f) &= \log \mathbb{E}_{x, x^-} [\exp(-\|f(x) - f(x^-)\|^2 / 2\tau)] \\ L_{\text{same}}(f) &= \log \mathbb{E}_{x, x^+} [\exp(-\|f(x) - f(x^+)\|^2 / 2\tau)] \end{aligned}$$

Next, we apply Wang and Isola [42]'s approach from their Theorem 1 to analyze individual terms. For simplicity, we present the binary setting $K = 2$. We abuse notation and use f and μ , the pushforward measure of x on the hypersphere, interchangeably in $L_{\text{spread}}(f, \alpha)$ as well as in the loss components in Definition 1.

Proposition 1 (Individual losses). $L_{\text{align}}(f)$ and $L_{\text{aug}}(f)$ are minimized when $f(x) = f(x^+)$ and $f(x) = f(a(x))$ almost surely, respectively. $L_{\text{diff}}(\mu)$ is minimized when $\mu = \delta_v$. $L_{\text{same}}(\mu)$ is minimized when $\mu = \sigma_{d-1}$.

When $\alpha = 0$, the ‘‘active’’ loss terms are L_{align} and L_{diff} , whose optima are jointly realizable and yield $\mu = \delta_v$ overall. When $\alpha = 1$, the terms L_{aug} and L_{same} are also compatible, yielding $\mu = \sigma_{d-1}$ and augmentations with the same embedding as their original point.

Neither of these distributions has good coarse-to-fine transfer performance on its own: δ_v loses information within classes, and σ_{d-1} allows points of different classes to be close together (Figure 1 left). To avoid both δ_v and σ_{d-1} , $\alpha \in (0, 1)$ must achieve a balance between the two loss terms. But the behavior of the weighted loss overall is unclear from the result in Proposition 1. It is also unclear whether there even exists an intermediate distribution that minimizes $L_{\text{spread}}(\mu, \alpha)$.

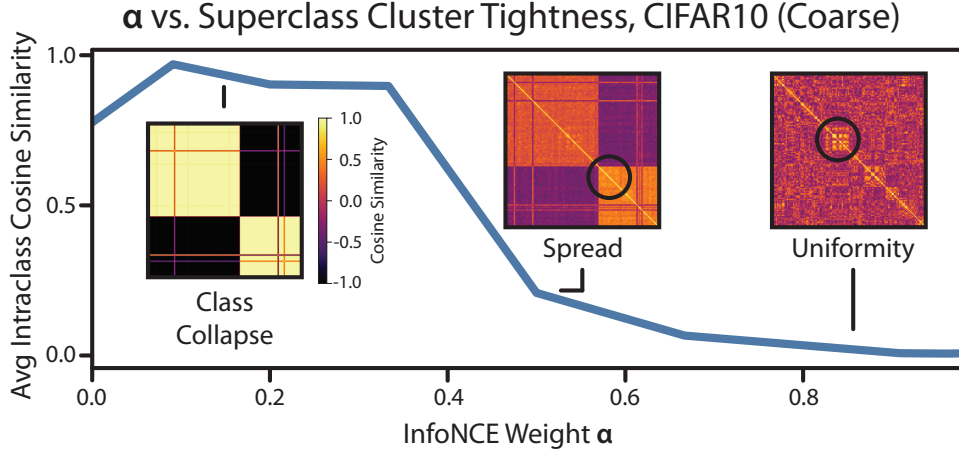


Figure 2: Measure of cluster tightness vs. α . Clusters are collapsed for low values of α , display spread for a small region, and then dissolve into uniformity for high values of α . Inserts: heatmaps of cosine similarity between points, sorted by class and subclass. Circles: apparent subclass clusters within spread.

3.3 Our Spread Result

We seek to analyze the geometry of the overall loss. Explicitly characterizing the optimal geometry is challenging, so we design a family of measures on the hypersphere and examine when such measures obtain lower loss than collapsed or uniform measures.

We assign mass evenly on two points that are close to v_y , a vertex of the regular simplex, but separated by some angle θ for each μ_y (see Figure 4 in Appendix H). Formally, define a block-diagonal rotation matrix $R_\theta \in \mathbb{R}^{d \times d}$ consisting of submatrices $\begin{bmatrix} \cos \theta & -\sin \theta \\ \sin \theta & \cos \theta \end{bmatrix}$ and I_{d-2} on the diagonal. For $\theta \in (0, \pi/2]$, define the measure $\mu_\theta = \{\mu_{0,\theta}, \mu_{1,\theta}\}$, where $\mu_{0,\theta} = \frac{1}{2}\delta_{R_\theta v_0} + \frac{1}{2}\delta_{R_{-\theta} v_0}$, and similarly $\mu_{1,\theta} = \frac{1}{2}\delta_{R_\theta v_1} + \frac{1}{2}\delta_{R_{-\theta} v_1}$. We present a technical result on the range of α for which μ_θ attains lower loss than class-collapsed or class-uniform measures.

Theorem 2. Let $c_{\tau,d} = \frac{2 + \frac{1}{\tau} - \sqrt{\frac{1}{\tau}(-2 + \frac{1}{\tau}) - 2 \log W_{1/2\tau}(\mathcal{S}^{d-1})}}{3}$, where $W_{1/2\tau}(\mathcal{S}^{d-1})$ is a constant depending on τ and d (see Appendix C.1 for exact value). Then, when $\alpha \in (2/3, c_{\tau,d})$, $\theta^* = \arcsin \sqrt{\frac{\tau}{2} \log \frac{3\alpha-1}{3-3\alpha}}$ minimizes $L_{\text{spread}}(\mu_\theta, \alpha)$ and satisfies $L_{\text{spread}}(\mu_{\theta^*}, \alpha) \leq \min_{\mu \in \{\delta_v, \sigma_{d-1}\}} L_{\text{spread}}(\mu, \alpha)$.

Our result does not define the exact optimal geometry since it constrains the measures we optimize to μ_θ . For $\alpha \notin (2/3, c_{\tau,d})$, it also does not specify the optimal geometry—we only know that the optimal geometry is not μ_θ .

However, our result yields a high-level insight: there exists a range of α for which the optimal geometry that minimizes $L_{\text{spread}}(\mu, \alpha)$ spreads out points on the hypersphere. Concretely, define the spread of class y under f as $s_f(y) = \mathbb{E}_{h(x)=y} [\|f(x) - \mathbb{E}_{h(x)=y}[f(x)]\|]$.

Corollary 1. If $\alpha \in (2/3, c_{\tau,d})$ and $f(x)$ has measure μ_{θ^*} , the spread for y under f is $s_f(y) = \sqrt{\frac{\tau}{2} \log \frac{3\alpha-1}{3-3\alpha}} \sim \omega(1)$.

In other words, L_{spread} can yield an extent of spread $s_f(y)$ that is controlled by α . Experiments on CIFAR10 support our result (Figure 2); the geometry is collapsed for low values of α , followed by a region of spread, followed by uniformity.

Finally, we remark on two deliberate aspects of our analysis. First, to avoid issues of non-convexity, we directly compare the overall loss of our measures with those of the two extrema δ_v and σ_{d-1} . Second, general distributions beyond the regular simplex and normalized surface measure are hard to compute contrastive losses over, and such computations are not largely studied to the extent of our knowledge. This inherently restricts analysis to simple distributions like μ_θ .

4 Breaking Permutation Invariance

Our analysis in the previous section shows that L_{spread} can obtain an optimal geometry that is neither collapsed nor uniform. However, this result does not completely explain improved transfer performance because L_{spread} under the previous setup is *class-fixing permutation invariant*, a property we define in Section 4.1. Inducing an inductive bias can break such an invariance. We argue that an inductive bias that encourages clustering of latent subclasses can be particularly useful. In Section 4.2, we show that generalization error on coarse-to-fine transfer learning depends on both $s_f(y)$ and a notion of subclass clustering $\sigma_f(z)$. We thus discuss three approaches for controlling $\sigma_f(z)$: one standard, and two alternatives with more realistic assumptions (Section 4.3).

4.1 Class-Fixing Permutation Invariance

First, we define class-fixing permutation invariance.

Definition 2 (Class-Fixing Permutation Invariance). *Let \mathcal{F} be a class of encoders. Let $L(f, B)$ be a loss function over an encoder $f \in \mathcal{F}$ and a set of n points $B = \{x_1, \dots, x_n\}$. Define $S_{h,B}$ as the set of class-fixing permutations such that $\pi \in S_{h,B} : [n] \rightarrow [n]$ satisfies $h(x_{\pi(i)}) = h(x_i)$ for all $i \in [n]$. Then, L is invariant on class-fixing permutations under \mathcal{F} if, for any batch B , permutation $\pi \in S_{h,B}$, and encoder $f \in \mathcal{F}$, there exists another encoder $f^\pi \in \mathcal{F}$ such that $f^\pi(x_i) = f(x_{\pi(i)})$ for all $i \in [n]$ and $L(f, B) = L(f^\pi, B)$.*

We find that L_{spread} is invariant on class-fixing permutations under the infinite encoder assumption from Section 2.3.

Proposition 2. *Let \mathcal{F} be the set of infinite encoders. Then L_{spread} is invariant on class-fixing permutations under \mathcal{F} .*

Under class-fixing permutation invariance, data points can be arbitrarily mapped to representations within their classes, suggesting that the mapping that minimizes L_{spread} is not unique. However, not all these mappings achieve the same performance on downstream tasks. Therefore, while our result from Section 3 provides insight into L_{spread} 's geometry under an infinitely powerful encoder, it cannot completely explain representation quality.

4.2 Inductive Bias for Improved Coarse-to-fine Transfer

Inducing an inductive bias can break permutation invariance (see Lemma 4 in the Appendix for a simple example). We argue that inducing subclass clustering can be particularly helpful for transfer performance. We measure subclass clustering in embedding space via the expected distance to the center of the subclass, $\sigma_f(z) = \mathbb{E}_{x \sim \mathcal{P}_z} [\|f(x) - \mathbb{E}_{x \sim \mathcal{P}_z} [f(x)]\|]$. We show that this quantity $\sigma_f(z)$, along with degree of spread $s_f(y)$, is critical for the generalization error of coarse-to-fine transfer.

To present our result on coarse-to-fine generalization error, we define some additional terms. Let y denote the class label of z . Define the quantity $\delta_f(z, z') = \frac{1}{p(z|y)p(z'|y)} (s_f(y) - p(z|y)^2 \sigma_f(z) - p(z'|y)^2 \sigma_f(z'))$ as a notion of separation between z and z' . $\delta_f(z, z')$ is large when there is spread (large $s_f(y)$) and sufficient subclass clustering (low $\sigma_f(z), \sigma_f(z')$). Define the variance of a subclass as $\text{Var}_f[z] = \mathbb{E}_{x \sim \mathcal{P}_z} [\|f(x) - \mathbb{E}_{x \sim \mathcal{P}_z} [f(x)]\|^2]$. We assume that for all $x \sim \mathcal{P}_z$, there exists a $c > 0$ such that $\|f(x) - \mathbb{E}_{x \sim \mathcal{P}_z} [f(x)]\| \geq c \cdot \mathbb{E}_{x \sim \mathcal{P}_z, x' \sim \mathcal{P}_{z'}} [\|f(x) - f(x')\|]$ (i.e., no point from z is equal to the center of z').

Theorem 3. *Denote $r_f(z, z') = c^2 \delta_f(z, z')^2 - |\text{Var}_f[z] - \text{Var}_f[z']|$. With probability $1 - \delta$, the coarse-to-fine error is at most*

$$L_{\gamma, f}(z) \leq \frac{\sigma_f(z)}{\sqrt{r_f(z, z') - 2 \log \gamma}} + \mathcal{O}\left(\left(\frac{d \log(d/\delta)}{m_z \wedge m_{z'}}\right)^{1/4}\right).$$

under the boundary condition that $r_f(z, z') - 2 \log \gamma \geq 16 \sqrt{\frac{2d \log(8d/\delta)}{m_z \wedge m_{z'}}} + \frac{2d \log(8d/\delta)}{m_z}$.

The generalization error depends on the sampling error, γ , and quantities intrinsic to the distribution of $f(x)$:

Table 1: Three mechanisms for inductive bias and empirical measurements of their associated Lipschitzness constants. Higher K is a worse Lipschitzness constant, which suggests the assumptions are less realistic

Mechanism	Assumptions	Lipschitzness Constant
Encoder (Constrained)	Lipschitz f	$K_L = 0.058$
Autoencoder	Decoder g reverse Lipschitz	$K_g = 0.041$
Augmentations	Lipschitz f on augmentations	$K_{aug} = 0.040$

- $s_f(y)$: the bound scales inversely in $s_f(y)$; points in a class must be spread out in order for subclasses to be distinguishable. Corollary 1 and empirical measurements (Figure 2) suggest that spread is non-zero when using L_{spread} with α set properly. Note that under SupCon, $s_f(y)$ is asymptotically equal to 0 and this bound is vacuous (refer to Theorem 1 for SupCon’s generalization error).
- $\sigma_f(z)$: the bound scales in $\sigma_f(z)$, confirming that spread alone is insufficient. Subclasses also need to be clustered tightly to achieve good transfer performance.
- $|\text{Var}_f[z] - \text{Var}_f[z']|$: distinguishing z versus z' may be difficult when only one subclass is clustered. When both $\sigma_f(z)$ and $\sigma_f(z')$ are small, this quantity is negligible.

Altogether, the generalization error scales in $\frac{\sigma_f(z)}{s_f(y)}$. Therefore, in addition to having sufficient spread $s_f(y)$, it is critical that $\sigma_f(z)$ is bounded. We thus explore techniques for inducing an inductive bias that can control this quantity.

4.3 Techniques for Inducing Subclass Clustering

We analyze three mechanisms on f for inducing an inductive bias that can cluster subclasses: a constrained encoder, a class-conditional autoencoder, and data augmentations. These three mechanisms use Lipschitzness assumptions of varying strength to bound $\sigma_f(z)$. We assume that subclasses are “clustered” in input space; i.e. there exists some σ_z such that $\mathbb{E}_{x, x' \sim \mathcal{P}_z} [\|x - x'\|] \leq \sigma_z$, and we study how these mechanisms on f allow us to control $\sigma_f(z)$ in terms of σ_z . For each mechanism, we show that $\sigma_f(z) \sim K\sigma_z$ for some particular Lipschitzness constant K . The lower the Lipschitzness constant, the better each mechanism can induce subclass clustering.

We summarize the assumptions of each mechanism in Section 4.3.4 and report empirical estimates of Lipschitz constants in Table 1. Section 4.3.4 also reports estimates of $\frac{\sigma_f(z)}{s_f(y)}$, the ratio that governs the generalization error in Theorem 3, showing how these mechanisms impact this quantity.

4.3.1 Lipschitz Encoder

One common method for inducing bias is constraining the class of encoders \mathcal{F} to be Lipschitz smooth. We show that restricting \mathcal{F} to the class of K_L -Lipschitz encoders encourages subclass clustering in representation space.

Lemma 1. *Let \mathcal{F}_{K_L} be the class of K_L -Lipschitz encoders. Then for any $f_{K_L} \in \mathcal{F}_{K_L}$, $\sigma_{f_{K_L}}(z) \leq K_L\sigma_z$.*

Lipschitzness with a sufficiently low constant K_L is realistic for simple function classes, such as MLPs with bounded norms. However, modern deep networks are not Lipschitz, as they are powerful enough to memorize random noise [44]. In Table 1 we confirm that the Lipschitz constant estimated empirically from our model’s encoder on real data is relatively high. Therefore, since encoders with deep architectures are not Lipschitz, we consider other more realistic methods and assumptions that can encourage subclass clustering.

4.3.2 Class-Conditional Autoencoder

To encourage embeddings to preserve properties of the input space without assuming Lipschitzness over the encoder, we propose concatenating embeddings from separate “class-conditional” autoencoders, each consisting of an encoder $f_{AE} \in \mathcal{F}_{AE}$ and a decoder $g \in \mathcal{G}$, to the embeddings learned from L_{spread} . An autoencoder for class y aims to

minimize the class reconstruction loss $\hat{L}_{AE}(\mathcal{D}_y) = \frac{1}{n_y} \sum_{x \in \mathcal{D}_y} \|g(f_{AE}(x)) - x\|^2$. These K per-class autoencoders thus intuitively learn distinctions within classes.

Define a notion of Rademacher complexity $\mathfrak{R}_n^p(\mathcal{F}_1, \mathcal{F}_2) = \mathbb{E}_\sigma \left[\sup_{f_1, f_2 \in \mathcal{F}_1, \mathcal{F}_2} \frac{1}{n} \sum_{i=1}^n \sigma_i \|f_1(x_i) - f_2(x_i)\|^p \right]$ for Rademacher random variables $\sigma = \{\sigma_1, \dots, \sigma_n\}$.

Lemma 2. *For any $g \in \mathcal{G}$, suppose there exists a $K_g > 0$ such that g is “reverse Lipschitz”, satisfying $\|f_{AE}(x) - f_{AE}(x')\| \leq K_g \|g(f_{AE}(x)) - g(f_{AE}(x'))\|$, and there exists finite b such that the reconstruction loss satisfies $\max_x \|g(f_{AE}(x)) - x\|^2 \leq b$.*

Then with probability at least $1 - \delta$,

$$\sigma_{f_{AE}}(z) \leq \frac{2K_g}{p(z|y)} \left(\hat{L}_{AE}(\mathcal{D}_y) + 2\mathfrak{R}_{n_y}^2(\mathcal{G} \circ \mathcal{F}_{AE}, id_{\mathcal{X}}) + b\sqrt{\log(1/\delta)/2n_y} \right)^{1/2} + K_g \sigma_z, \quad (4)$$

where $id_{\mathcal{X}}$ is the identity function on \mathcal{X} , and $p(z|y) = \frac{p(z)}{p(y)}$ is the probability that x drawn from $p(\cdot|y)$ has label z .

There are no explicit assumptions on f_{AE} ; instead, a condition on the decoder is used for clustering subclasses. In Appendix C.2, we show that for an autoencoder trained on \mathcal{D} instead of \mathcal{D}_y , $p(z)$ replaces $p(z|y)$, and n replaces n_y . That is, while a general autoencoder is learned on more data, individual subclasses comprise a smaller proportion of the data and thus could be harder to learn meaningful representations of. This suggests that $\sigma_{f_{AE}}(z)$ is roughly a constant factor larger with a general autoencoder when n_y and n are both large, and thus a class-conditional autoencoder can better cluster subclasses.

4.3.3 Data Augmentation

Another way of inducing inductive bias for subclass clustering is data augmentations, which we use in L_{spread} and which play a prominent role in contrastive learning overall. Define $\mathcal{A} : \mathcal{X} \rightarrow \mathcal{X}$ as the function class of augmentations and \mathcal{F}_{aug} as the class of encoders.

Lemma 3. *For $a \in \mathcal{A}$ and any $x, x' \in \mathcal{X}$, suppose that $f_{aug} \in \mathcal{F}_{aug}$ satisfies $\|f_{aug}(a(x)) - f_{aug}(a(x'))\| \leq K_{aug} \|a(x) - a(x')\|$ for some K_{aug} and that $f(a(x)) = f(x)$ for $x \in \mathcal{D}$. Denote $\sigma_z^{aug} = \mathbb{E}_{x, x' \sim \mathcal{P}_z} [\|a(x) - a(x')\|]$. Then with probability at least $1 - \delta$,*

$$\sigma_{f_{aug}}(z) \leq \frac{2}{p(z)} \left(2\mathfrak{R}_n^1(\mathcal{F}_{aug}, \mathcal{F}_{aug} \circ \mathcal{A}) + \sqrt{2 \log(1/\delta)/n} \right) + K_{aug} \sigma_z^{aug}.$$

Our result assumes Lipschitzness only on the augmentations, which is consistent with literature such as Dao et al. [10], and that the model can align augmented and original training data pairs. $\sigma_f(z)$ scales with how close augmentations of points within a subclass are, σ_z^{aug} . This quantity can actually be less than σ_z under assumptions in prior work on characterizing augmentations [24], which results in tighter embedding clusters. Our result can also explain why prior works [25] observe that modified losses (that include augmentations) result in better transfer.

4.3.4 Overall Takeaways

Our results from Lemmas 1, 2, and 3 show that $\sigma_f(z)$, which is critical for transfer performance as demonstrated in Theorem 3, can be controlled. Table 1 summarizes our results on how a standard encoder, an autoencoder, and data augmentations can encourage subclass clustering under various assumptions. We report empirical measures of K_L , K_g and K_{aug} on real datasets, and find that the autoencoder and data augmentation assumptions are more realistic (lower values of K).

Figure 2 demonstrates these effects on real data; apparent clusters begin forming under L_{spread} (which is trained with data augmentation). We also measure the ratio $\frac{\sigma_f(z)}{\sigma_f(y)}$ and find that it can range as high as 1.94 for SupCon. For L_{spread} with augmentations and the autoencoder, the maximum values are 1.05 and 1.03, respectively—suggesting that these modifications control subclass clustering better, and should result in better coarse-to-fine transfer.

Table 2: Summary of the datasets we use for evaluation.

Dataset	K_{coarse}	K_{fine}	Notes
CIFAR10	2	10	Coarse labels are animal vs. vehicle
CIFAR100	20	100	Standard coarse labels
CIFAR100-U	20	100	CIFAR100, imbalanced fine classes
MNIST	2	10	Coarse labels are < 5 and ≥ 5
TinyImageNet	67	200	Coarse labels from ImageNet hierarchy
Waterbirds	2	3	Bird images [36]
ISIC	2	3	Skin lesions [9]
CelebA	2	3	Celebrity faces [31]

Table 3: Coarse-to-fine transfer learning performance. Best in bold.

Method		CIFAR10	CIFAR100	CIFAR100-U	MNIST	TinyImageNet
Baselines	InfoNCE [7]	77.6 ± 0.1	60.5 ± 0.1	56.4 ± 0.3	98.4 ± 0.1	44.9 ± 0.1
	SupCon [27]	51.8 ± 1.2	56.1 ± 0.1	49.8 ± 0.3	95.4 ± 0.1	43.9 ± 0.1
	SupCon + InfoNCE [25]	77.6 ± 0.1	55.7 ± 0.1	48.0 ± 0.2	98.6 ± 0.1	46.1 ± 0.1
Ours	cAuto	71.4 ± 0.1	62.9 ± 0.1	58.7 ± 0.5	98.7 ± 0.1	47.1 ± 0.1
	SupCon + cNCE (L_{spread})	77.1 ± 0.1	58.7 ± 0.2	53.5 ± 0.4	98.5 ± 0.1	45.8 ± 0.1
	SupCon + cAuto	71.7 ± 0.1	63.8 ± 0.6	59.8 ± 0.3	98.7 ± 0.1	49.3 ± 0.1
	SupCon + cNCE + cAuto (THANOS)	79.1 ± 0.2	65.0 ± 0.2	59.7 ± 0.3	99.0 ± 0.1	49.6 ± 0.1

5 Experiments

In this section, we evaluate how well adding a class-conditional InfoNCE loss and a class-conditional autoencoder improves the representations produced by supervised contrastive learning. We call our overall method **THANOS**. This section is primarily designed to evaluate two claims:

- We use coarse-to-fine transfer learning to evaluate how well the representations maintain subclass information. **THANOS** achieves 11.1 lift on average across five datasets.
- We evaluate how well **THANOS** can improve worst-group robustness in the unlabeled setting. **THANOS** detects low-performing sub-groups 6.2 points better than SupCon across three datasets. **THANOS** sets state-of-the-art worst-group robustness without sub-group labels by 11.5 points on CelebA—and even outperforms an algorithm that has access to ground-truth sub-group labels in some cases.

We also present ablations. Additional experiments on overall model quality are in Appendix G. Although we focus on coarse-to-fine transfer and robustness here, we note that our method also produces lift on overall model quality.

THANOS Method We summarize the **THANOS** method. **THANOS** consists of adding a class-conditional InfoNCE loss and a class-conditional autoencoder to the supervised contrastive loss. We implement the former by training an encoder with L_{spread} . To implement the latter, we train a single autoencoder with a joint MSE reconstruction loss and a cross entropy loss. We then concatenate the autoencoder representation to the representation of the encoder trained with L_{spread} . Details on architectures and hyperparameters in Appendix F.

Datasets Table 2 lists the datasets we use in our evaluation. We use coarse versions of CIFAR10, CIFAR100, MNIST, and TinyImageNet to study coarse-to-fine transfer. We use Waterbirds, ISIC and CelebA for robustness [36, 9, 31, 37].

Coarse-to-Fine Transfer We use coarse-to-fine transfer learning to isolate how well representations separate subclasses in an ideal setting. We train models on coarse labels, freeze the weights, and then train a linear probe over

Table 4: Unsupervised subclass recovery (top, F1), and worst-group performance (AUROC for ISIC, Acc for others). Best in bold.

Method	Group Labels	Waterbirds	ISIC	CelebA
Sub-Group Recovery				
Sohoni et al. [37]	✗	56.3	74.0	24.2
SupCon	✗	47.1	92.5	19.4
THANOS	✗	59.0	93.8	24.8
Worst-Group Robustness				
Sohoni et al. [37]	✗	88.4	92.0	55.0
JTT [30]	✗	83.8	91.8	77.9
SupCon	✗	86.8	93.3	66.1
THANOS	✗	88.6	92.6	89.4
GroupDRO	✓	90.7	92.3	88.9

the final layer on fine labels. For the autoencoder experiments, we train an autoencoder separately and concatenate its embedding layer with the contrastive embedding for the linear probe. We jointly optimize all contrastive losses and the class-conditional autoencoder with a cross-entropy loss head. We train all models with dropout as well as label smoothing on the cross-entropy loss heads.

We report four variants of THANOS: the class-conditional autoencoder on its own, SupCon modified with a class-conditional InfoNCE loss, SupCon modified with a class-conditional autoencoder, and SupCon with both modifications. We report 3 baselines from previous work on the transferability of SupCon [25]: SupCon, SupCon plus an InfoNCE loss, and the InfoNCE loss on its own.

THANOS significantly outperforms SupCon on coarse-to-fine transfer learning—by an average of 11.1 points across all tasks. 7.3 points can be attributed to the class-conditional InfoNCE loss on average, but mileage varies between tasks (25.3 points of lift for CIFAR10, vs. 2.6 for CIFAR100). The difference is the number of coarse classes: CIFAR10 only has two coarse classes, whereas CIFAR100 has 20. Fewer coarse classes makes it easier to achieve class collapse, so spread is more necessary. Finally, we also note that combining the autoencoder with the other components outperforms using the autoencoder on its own, by 2.7 points on average. This suggests that each component is helpful.

Worst-Group Robustness We use robustness to measure how well THANOS can recover hidden subgroups in an unsupervised setting. For these models, we train contrastive losses on their own. We follow the methodology from Sohoni et al. [37]. We first train a model with class labels. We then cluster the embeddings to produce pseudolabels for subclasses, which we use as input to the GroupDRO algorithm to optimize worst-group robustness [36].

We compare subgroup recovery against SupCon and Sohoni et al. [37]. We compare worst-group robustness against Sohoni et al. [37] and JTT [30], as well as using sub-group labels from SupCon. We also report the performance of GroupDRO with ground-truth subclass labels.

Table 4 shows the results. THANOS outperforms both SupCon and Sohoni et al. [37] on subgroup recovery. THANOS further achieves state-of-the-art worst-group robustness, outperforming JTT by 4.7 points and Sohoni et al. [37] by 11.7 points on average—and setting state-of-the-art on CelebA by 11.5 points. Surprisingly, THANOS can even outperform GroupDRO with ground-truth subclass labels in two cases.

Ablations We summarize two ablations (Appendix G.3). First, we validate Lemma 2 and find that using a generic autoencoder underperforms a class-conditional autoencoder by 30.0 points on average—and furthermore does not improve the performance of SupCon as well (2.0 points of lift compared to 11.0 points). Second, we validate Lemma 3 and confirm that data augmentation is crucial; removing data augmentation degrades performance by 35.4 points.

6 Related Work and Discussion

We present an abbreviated related work. A full treatment can be found in Appendix A. Our theoretical work relates to theory on the geometry of contrastive learning [42, 19, 35, 46], collapsed representations [16, 26], autoencoders [14, 28], data augmentation [21, 20, 1], and robustness [37]. Our use of L_{spread} and an autoencoder draws from a wave of empirical work on contrastive learning [7, 27], and its properties [25, 5].

In aggregate, we study how to improve the quality of representations trained with supervised contrastive learning. We identify controlling spread and inducing subclass clustering as two key challenges and show how two modifications to supervised contrastive learning improve transfer and robustness.

Authors' Note

The first two authors contributed equally. Co-first authors can prioritize their names when adding this paper's reference to their resumes.

Acknowledgments

We thank Beidi Chen, Tri Dao, Karan Goel, and Albert Gu for their helpful comments on early drafts of this paper. We gratefully acknowledge the support of NIH under No. U54EB020405 (Mobilize), NSF under Nos. CCF1763315 (Beyond Sparsity), CCF1563078 (Volume to Velocity), and 1937301 (RTML); ONR under No. N000141712266 (Unifying Weak Supervision); ONR N00014-20-1-2480: Understanding and Applying Non-Euclidean Geometry in Machine Learning; N000142012275 (NEPTUNE); the Moore Foundation, NXP, Xilinx, LETI-CEA, Intel, IBM, Microsoft, NEC, Toshiba, TSMC, ARM, Hitachi, BASF, Accenture, Ericsson, Qualcomm, Analog Devices, the Okawa Foundation, American Family Insurance, Google Cloud, Salesforce, Total, the HAI-GCP Cloud Credits for Research program, the Stanford Data Science Initiative (SDSI), Department of Defense (DoD) through the National Defense Science and Engineering Graduate Fellowship (NDSEG) Program, and members of the Stanford DAWN project: Facebook, Google, and VMWare. The Mobilize Center is a Biomedical Technology Resource Center, funded by the NIH National Institute of Biomedical Imaging and Bioengineering through Grant P41EB027060. The U.S. Government is authorized to reproduce and distribute reprints for Governmental purposes notwithstanding any copyright notation thereon. Any opinions, findings, and conclusions or recommendations expressed in this material are those of the authors and do not necessarily reflect the views, policies, or endorsements, either expressed or implied, of NIH, ONR, or the U.S. Government.

References

- [1] Mahdi Abavisani, Alireza Naghizadeh, Dimitris N Metaxas, and Vishal M Patel. Deep subspace clustering with data augmentation. In *Thirty-fourth Conference on Neural Information Processing Systems*, 2020.
- [2] Sanjeev Arora, Hrishikesh Khandeparkar, Mikhail Khodak, Orestis Plevrakis, and Nikunj Saunshi. A theoretical analysis of contrastive unsupervised representation learning. *arXiv preprint arXiv:1902.09229*, 2019.
- [3] Sergiy V Borodachov, Douglas P Hardin, and Edward B Saff. *Discrete energy on rectifiable sets*. Springer, 2019.
- [4] Mike Bostock. Imagenet hierarchy, 2018. URL <https://observablehq.com/@mbostock/imagenet-hierarchy>.
- [5] Guy Bukchin, Eli Schwartz, Kate Saenko, Ori Shahar, Rogerio Feris, Raja Giryes, and Leonid Karlinsky. Fine-grained angular contrastive learning with coarse labels. In *2021 IEEE/CVF Conference on Computer Vision and Pattern Recognition (CVPR)*. IEEE, Jun 2021.

- [6] Mathilde Caron, Ishan Misra, Julien Mairal, Priya Goyal, Piotr Bojanowski, and Armand Joulin. Unsupervised learning of visual features by contrasting cluster assignments. In *Advances in Neural Information Processing Systems*, 2020.
- [7] Ting Chen, Simon Kornblith, Mohammad Norouzi, and Geoffrey Hinton. A simple framework for contrastive learning of visual representations. In *International conference on machine learning*. PMLR, 2020.
- [8] Xinlei Chen, Haoqi Fan, Ross Girshick, and Kaiming He. Improved baselines with momentum contrastive learning. *arXiv preprint arXiv:2003.04297*, 2020.
- [9] Noel Codella, Veronica Rotemberg, Philipp Tschandl, M Emre Celebi, Stephen Dusza, David Gutman, Brian Helba, Aadi Kallou, Konstantinos Liopyris, Michael Marchetti, et al. Skin lesion analysis toward melanoma detection 2018: A challenge hosted by the international skin imaging collaboration (isic). *arXiv preprint arXiv:1902.03368*, 2019.
- [10] Tri Dao, Albert Gu, Alexander Ratner, Virginia Smith, Chris De Sa, and Christopher Ré. A kernel theory of modern data augmentation. In Kamalika Chaudhuri and Ruslan Salakhutdinov, editors, *Proceedings of the 36th International Conference on Machine Learning*, volume 97 of *Proceedings of Machine Learning Research*, pages 1528–1537. PMLR, 09–15 Jun 2019.
- [11] Greg d’Eon, Jason d’Eon, James R Wright, and Kevin Leyton-Brown. The spotlight: A general method for discovering systematic errors in deep learning models. *arXiv preprint arXiv:2107.00758*, 2021.
- [12] Alexey Dosovitskiy, Lucas Beyer, Alexander Kolesnikov, Dirk Weissenborn, Xiaohua Zhai, Thomas Unterthiner, Mostafa Dehghani, Matthias Minderer, Georg Heigold, Sylvain Gelly, et al. An image is worth 16x16 words: Transformers for image recognition at scale. In *International Conference on Learning Representations*, 2020.
- [13] John Duchi, Tatsunori Hashimoto, and Hongseok Namkoong. Distributionally robust losses for latent covariate mixtures. *arXiv preprint arXiv:2007.13982*, 2020.
- [14] Baruch Epstein and Ron Meir. Generalization bounds for unsupervised and semi-supervised learning with autoencoders. *arXiv preprint arXiv:1902.01449*, 2019.
- [15] William Falcon and Kyunghyun Cho. A framework for contrastive self-supervised learning and designing a new approach. *arXiv preprint arXiv:2009.00104*, 2020.
- [16] Tomer Galanti, András György, and Marcus Hutter. On the role of neural collapse in transfer learning. *arXiv preprint arXiv:2112.15121*, 2021.
- [17] Karan Goel, Albert Gu, Yixuan Li, and Christopher Re. Model patching: Closing the subgroup performance gap with data augmentation. In *International Conference on Learning Representations*, 2020.
- [18] Priya Goyal, Mathilde Caron, Benjamin Lefaudeaux, Min Xu, Pengchao Wang, Vivek Pai, Mannat Singh, Vitaliy Liptchinsky, Ishan Misra, Armand Joulin, et al. Self-supervised pretraining of visual features in the wild. *arXiv preprint arXiv:2103.01988*, 2021.
- [19] Florian Graf, Christoph Hofer, Marc Niethammer, and Roland Kwitt. Dissecting supervised contrastive learning. In *International Conference on Machine Learning*, pages 3821–3830. PMLR, 2021.
- [20] Xifeng Guo, En Zhu, Xinwang Liu, and Jianping Yin. Deep embedded clustering with data augmentation. In *Asian conference on machine learning*, pages 550–565. PMLR, 2018.
- [21] Jeff Z HaoChen, Colin Wei, Adrien Gaidon, and Tengyu Ma. Provable guarantees for self-supervised deep learning with spectral contrastive loss. *arXiv preprint arXiv:2106.04156*, 2021.
- [22] Kaiming He, Haoqi Fan, Yuxin Wu, Saining Xie, and Ross Girshick. Momentum contrast for unsupervised visual representation learning. *arXiv preprint arXiv:1911.05722*, 2019.

- [23] Achim Hoffmann, Rex Kwok, and Paul Compton. Using subclasses to improve classification learning. In *European Conference on Machine Learning*, pages 203–213. Springer, 2001.
- [24] Weiran Huang, Mingyang Yi, and Xuyang Zhao. Towards the generalization of contrastive self-supervised learning, 2021.
- [25] Ashraful Islam, Chun-Fu Chen, Rameswar Panda, Leonid Karlinsky, Richard Radke, and Rogerio Feris. A broad study on the transferability of visual representations with contrastive learning. *arXiv preprint arXiv:2103.13517*, 2021.
- [26] Li Jing, Pascal Vincent, Yann LeCun, and Yuandong Tian. Understanding dimensional collapse in contrastive self-supervised learning. *arXiv preprint arXiv:2110.09348*, 2021.
- [27] Prannay Khosla, Piotr Teterwak, Chen Wang, Aaron Sarna, Yonglong Tian, Phillip Isola, Aaron Mschiot, Ce Liu, and Dilip Krishnan. Supervised contrastive learning. In *Thirty-Fourth Conference on Neural Information Processing Systems*, 2020.
- [28] Lei Le, Andrew Patterson, and Martha White. Supervised autoencoders: Improving generalization performance with unsupervised regularizers. In *Thirty-second Conference on Neural Information Processing Systems*, 2018.
- [29] Ya Le and Xuan Yang. Tiny imagenet visual recognition challenge. *CS 231N*, 7(7):3, 2015.
- [30] Evan Z Liu, Behzad Haghgoo, Annie S Chen, Aditi Raghunathan, Pang Wei Koh, Shiori Sagawa, Percy Liang, and Chelsea Finn. Just train twice: Improving group robustness without training group information. In *International Conference on Machine Learning*, pages 6781–6792. PMLR, 2021.
- [31] Ziwei Liu, Ping Luo, Xiaogang Wang, and Xiaoou Tang. Deep learning face attributes in the wild. In *Proceedings of International Conference on Computer Vision (ICCV)*, December 2015.
- [32] Mehryar Mohri, Afshin Rostamizadeh, and Ameet Talwalkar. *Foundations of machine learning*. MIT press, 2018.
- [33] Luke Oakden-Rayner, Jared Dunnmon, Gustavo Carneiro, and Christopher Ré. Hidden stratification causes clinically meaningful failures in machine learning for medical imaging. In *Proceedings of the ACM conference on health, inference, and learning*, pages 151–159, 2020.
- [34] Aaron van den Oord, Yazhe Li, and Oriol Vinyals. Representation learning with contrastive predictive coding. *arXiv preprint arXiv:1807.03748*, 2018.
- [35] Joshua Robinson, Ching-Yao Chuang, Suvrit Sra, and Stefanie Jegelka. Contrastive learning with hard negative samples. *arXiv preprint arXiv:2010.04592*, 2020.
- [36] Shiori Sagawa, Pang Wei Koh, Tatsunori B Hashimoto, and Percy Liang. Distributionally robust neural networks for group shifts: On the importance of regularization for worst-case generalization. In *International Conference on Learning Representations*, 2019.
- [37] Nimit Sohoni, Jared Dunnmon, Geoffrey Angus, Albert Gu, and Christopher Ré. No subclass left behind: Fine-grained robustness in coarse-grained classification problems. *Thirty-fourth Conference on Neural Information Processing Systems*, 2020.
- [38] J. J. Thomson. XI. cathode rays. *The London, Edinburgh, and Dublin Philosophical Magazine and Journal of Science*, 44(269):293–316, 1897.
- [39] Yonglong Tian, Chen Sun, Ben Poole, Dilip Krishnan, Cordelia Schmid, and Phillip Isola. What makes for good views for contrastive learning? *arXiv preprint arXiv:2005.10243*, 2020.

- [40] Yao-Hung Hubert Tsai, Yue Wu, Ruslan Salakhutdinov, and Louis-Philippe Morency. Self-supervised learning from a multi-view perspective. In *International Conference on Learning Representations*, 2020.
- [41] Michael Tschannen, Josip Djolonga, Paul K. Rubenstein, Sylvain Gelly, and Mario Lucic. On mutual information maximization for representation learning. In *International Conference on Learning Representations*, 2020.
- [42] Tongzhou Wang and Phillip Isola. Understanding contrastive representation learning through alignment and uniformity on the hypersphere. In *International Conference on Machine Learning*, pages 9929–9939. PMLR, 2020.
- [43] P. Welinder, S. Branson, T. Mita, C. Wah, F. Schroff, S. Belongie, and P. Perona. Caltech-UCSD Birds 200. Technical Report CNS-TR-2010-001, California Institute of Technology, 2010.
- [44] Chiyuan Zhang, Samy Bengio, Moritz Hardt, Benjamin Recht, and Oriol Vinyals. Understanding deep learning requires rethinking generalization. In *International Conference on Learning Representations*, 2016.
- [45] Bolei Zhou, Agata Lapedriza, Jianxiong Xiao, Antonio Torralba, and Aude Oliva. Learning deep features for scene recognition using places database. *Twenty-eighth Conference on Neural Information Processing Systems*, 2014.
- [46] Roland S. Zimmermann, Yash Sharma, Steffen Schneider, Matthias Bethge, and Wieland Brendel. Contrastive learning inverts the data generating process. *arXiv preprint arXiv:2012.08850*, 2021.

We present a full treatment of related work in Appendix A. We present a glossary in Appendix B. We present proofs in Appendix C, additional theoretical results in Appendix D, and auxiliary lemmas in Appendix E. We present additional experimental details in Appendix F, additional results in Appendix G, and synthetics in Appendix H.

A Related Work

We presented an extended treatment of related work.

From work in contrastive learning, we take inspiration from Arora et al. [2], who use a latent classes view to study self-supervised contrastive learning. Similarly, Zimmermann et al. [46] considers how minimizing the InfoNCE loss recovers a latent data generating model. Recent work has also analyzed contrastive learning from the information-theoretic perspective [34, 39, 40], but does not fully explain practical behavior [41]. On the geometric side, we are inspired by the theoretical tools from Wang and Isola [42] and Graf et al. [19], who study representations on the hypersphere along with Robinson et al. [35]. There has also been work studying the properties of collapsed representations in transfer learning [16] and contrastive learning [26]. We offer another perspective on the relationship between collapse and embedding quality, and offer techniques to mitigate collapse.

Our work builds on the recent wave of empirical interest in contrastive learning [7, 22, 8, 18, 6] and supervised contrastive learning [27]. There has also been empirical work analyzing the transfer performance of contrastive representations and the role of intra-class variability in transfer learning. Islam et al. [25] find that combining supervised and self-supervised contrastive loss improves transfer learning performance, and they hypothesize that this is due to both inter-class separation and intra-class variability. Bukchin et al. [5] find that combining cross entropy and a class-conditional self-supervised contrastive loss improves coarse-to-fine transfer, also motivated by preserving intra-class variability.

Our use of L_{spread} and a class-conditional autoencoder arises from similar motivations to losses proposed in these works, and we further theoretically study their implications for spread. Our theoretical analysis of autoencoders draws from previous work [14, 28]. Our study of data augmentation similarly builds on recent theoretical analysis of the role of data augmentation in contrastive learning [21, 24] and clustering [20, 1].

Our treatment of subclasses is strongly inspired by Sohoni et al. [37] and Oakden-Rayner et al. [33], who document empirical consequences of hidden strata. We are inspired by empirical work that has demonstrated that detecting subclasses can be important for performance [23, 11] and robustness [13, 36, 17, 30].

B Glossary

The glossary is given in Table 5 below.

Symbol	Used for
x	Input data $x \in \mathcal{X}$ with distribution \mathcal{P} .
y	Class label $y \in \mathcal{Y} = \{0, \dots, K-1\}$, where $h(x)$ is x 's class label.
z	Latent subclass $z \in \mathcal{Z}$.
S_y	The set of all subclasses corresponding to class label y .
$p(z)$	The proportion of subclass z over \mathcal{Z} .
\mathcal{P}_z	The distribution of input data belonging to subclass z , i.e. $\mathcal{P}_z = p(\cdot z)$.
$S(z)$	The label corresponding to subclass z .
$h_s(x)$	The subclass that x belongs to.
\mathcal{D}	Training dataset of n points $\{(x_i, y_i)\}_{i=1}^n$.
\mathcal{D}_y	Training data with label y , $\mathcal{D}_y = \{x \in \mathcal{D} : h(x) = y\}$ of size n_y .
\mathcal{D}_z	Training data with latent subclass z , $\mathcal{D}_z = \{x \in \mathcal{D} : h_s(x) = z\}$ of size n_z .
f	The encoder $f : \mathcal{X} \rightarrow \mathbb{R}^d$ that maps input data to an embedding space with dimension d .
\mathcal{D}_s	A dataset of m points with subclass labels $\mathcal{D}_s = \{(x_i, z_i)\}_{i=1}^m$ used for coarse-to-fine transfer.
$\mathcal{D}_{s,z}$	The subset of \mathcal{D}_s with subclass z , $\mathcal{D}_{s,z} = \{x \in \mathcal{D}_s : h_s(x) = z\}$ of size m_z .
W_z	Linear weight W_z for model used in coarse-to-fine transfer.
$\hat{p}(z f(x))$	Softmax score output by linear model for coarse-to-fine transfer.
$L_{\gamma, f}(z)$	The γ -margin generalization error on subclass z in coarse-to-fine transfer.
B	Batch of input data.
$P(i, B)$	Points in B with the same label as x_i , $\{x^+ \in B \setminus i : h(x^+) = h(x_i)\}$.
$N(i, B)$	Points in B with a label different from that of x_i , $\{x^- \in B \setminus i : h(x^-) \neq h(x_i)\}$.
$a(x_i)$	An augmentation of x_i , where $a : \mathcal{X} \rightarrow \mathcal{X}$.
$\sigma_f(x, x')$	Notation for $\exp\left(\frac{f(x)^\top f(x')}{\tau}\right)$.
τ	Temperature hyperparameter in contrastive loss.
$L_{\text{spread}}(f, B)$	The contrastive loss we study (on batch B with encoder f), a weighted sum of a SupCon and class-conditional InfoNCE loss.
α	Weight parameter for L_{spread} .
L_{sup}	SupCon loss that is used in L_{spread} that pushes points of a class together (see (2)).
L_{cNCE}	Class-conditional InfoNCE loss that is used in L_{spread} to pull apart points within a class (see (3)).
\mathcal{S}^{d-1}	The unit hypersphere in \mathbb{R}^d .
μ_y	The pushforward measure of the class-conditional distribution $p(\cdot h(x) = y)$ via f , where $\mu_y \in \mathcal{M}(\mathcal{S}^{d-1})$, the set of all Borel probability measures on the hypersphere.
$\boldsymbol{\mu}$	$\boldsymbol{\mu} = \{\mu_y\}_{y \in \mathcal{Y}}$ is the overall pushforward measure $\mathcal{P} \circ f^{-1} \in \mathcal{M}(\mathcal{S}^{d-1})$.
\boldsymbol{v}	$\boldsymbol{v} = \{v_y\}_{y \in \mathcal{Y}} \in \mathcal{S}^{d-1}$ is the regular simplex inscribed in the hypersphere.
δ_{v_y}	The probability measure on \mathcal{S}^{d-1} with all mass on v_y .
$\boldsymbol{\delta}_v$	The class-collapsed measure $\boldsymbol{\delta}_v = \{\delta_{v_y}\}_{y \in \mathcal{Y}}$ where $f(x) = v_y$ almost surely whenever $h(x) = y$.
σ_{d-1}	The normalized surface area measure on \mathcal{S}^{d-1} .
$\boldsymbol{\sigma}_{d-1}$	The class-uniform measure where $\mu_y = \sigma_{d-1}$ for all $y \in \mathcal{Y}$.
f_{SC}	The encoder trained with SupCon, satisfying $f_{SC}(x) = v_y$ for all $x \in \mathcal{D}$ where $h(x) = y$.
x^+	Point for x 's positive pair, drawn from distribution $p(\cdot h(x^+) = h(x))$.
x^-	Point for x 's negative pair, drawn from distribution $p(\cdot h(x^-) \neq h(x))$.
$L_{\text{spread}}(f, \alpha)$	Asymptotic version of L_{spread} that we analyze (see Definition 1, also referred to as $L_{\text{spread}}(\boldsymbol{\mu}, \alpha)$).
R_θ	Rotation matrix $R_\theta \in \mathbb{R}^{d \times d}$ that rotates by angle θ in two dimensions.
$\boldsymbol{\mu}_\theta$	A measure $\boldsymbol{\mu}_\theta = \{\mu_{0,\theta}, \mu_{1,\theta}\}$ on the hypersphere that we compare against $\boldsymbol{\delta}_v$ and $\boldsymbol{\sigma}_{d-1}$. In particular, $\mu_{0,\theta} = \frac{1}{2} \delta_{R_\theta^\top v_0} + \frac{1}{2} \delta_{R_\theta^\top v_1}$ and similarly for $\mu_{1,\theta}$.
$c_{\tau, d}$	Constant that upper bounds the range of α for which some $\boldsymbol{\mu}_\theta$ attains lower $L_{\text{spread}}(\boldsymbol{\mu}, \alpha)$ than $\boldsymbol{\delta}_v$ or $\boldsymbol{\sigma}_{d-1}$.
$s_f(y)$	Notion of spread in embedding space, defined as $s_f(y) = \mathbb{E}_{h(x)=y} [\ f(x) - \mathbb{E}_{h(x)=y} [f(x)]\]$.
$\sigma_f(z)$	Notion of subclass clustering in embedding space, defined as $\sigma_f(z) = \mathbb{E}_{x \sim \mathcal{P}_z} [\ f(x) - \mathbb{E}_{x \sim \mathcal{P}_z} [f(x)]\]$.
$\text{Var}_f[z]$	Notion of subclass variance, defined as $\text{Var}_f[z] = \mathbb{E}_{x \sim \mathcal{P}_z} [\ f(x) - \mathbb{E}_{x \sim \mathcal{P}_z} [f(x)]\ ^2]$.
σ_z	How clustered a subclass is in input space, defined as $\sigma_z = \mathbb{E}_{x, x' \sim \mathcal{P}_z} [\ x - x'\]$.
K_L	The Lipschitzness constant of a Lipschitz encoder from function class \mathcal{F}_{K_L} .
f_{AE}, g	Autoencoder with encoder $f_{AE} \in \mathcal{F}_{AE}$ and decoder $g \in \mathcal{G}$.
\hat{L}_{AE}	The autoencoder's reconstruction loss (mean squared error).
$\mathfrak{R}_n^p(\mathcal{F}_1, \mathcal{F}_2)$	Notion of Rademacher complexity defined as $\mathfrak{R}_n^p(\mathcal{F}_1, \mathcal{F}_2) = \mathbb{E}_\sigma [\sup_{f_1, f_2 \in \mathcal{F}_1, \mathcal{F}_2} \frac{1}{n} \sum_{i=1}^n \sigma_i \ f_1(x_i) - f_2(x_i)\ ^p]$.
K_g	"Reverse Lipschitzness" constant of the decoder, e.g. $\ f_{AE}(x) - f_{AE}(x')\ \leq K_g \ g(f_{AE}(x)) - g(f_{AE}(x'))\ $.
\mathcal{A}	Function class of augmentations $\mathcal{A} : \mathcal{X} \rightarrow \mathcal{X}$.
\mathcal{F}_{aug}	Function class of encoders that are trained on augmentations.
K_a	The Lipschitzness constant on augmentations for $f_{aug} \in \mathcal{F}_{aug}$, e.g. $\ f_{aug}(a(x)) - f_{aug}(a(x'))\ \leq K_a \ a(x) - a(x')\ $ for any $x', x \in \mathcal{X}$ and $a \in \mathcal{A}$.
σ_z^{aug}	How clustered augmentations of a subclass are in input space.

Table 5: Glossary of variables and symbols used in this paper.

C Proofs

C.1 Proofs for Section 3

Theorem 1. For γ where $\log \gamma \geq 8 \max\{\mathfrak{R}_{n_z}(\mathcal{F}), \mathfrak{R}_{n_{z'}}(\mathcal{F})\}$, SupCon's coarse-to-fine error is at least

$$L_{\gamma, f_{SC}}(z) \geq 1 - \delta(n_z, \mathcal{F}, \gamma) - \delta(n_{z'}, \mathcal{F}, \gamma) - \xi(m_z \wedge m_{z'}, \gamma),$$

where $\delta(n_z, \mathcal{F}, \gamma) = d \exp\left(-\frac{n_z}{32d^2}(\log \gamma - 8\mathfrak{R}_{n_z}(\mathcal{F}))^2\right)$ bounds generalization error of f_{SC} and $\xi(m_z \wedge m_{z'}, \gamma) = 4d \exp\left(-\frac{(m_z \wedge m_{z'}) \log^2 \gamma}{32d}\right)$ bounds the noise from \mathcal{D}_s .

Proof. $L_{\gamma, f}(z) = \Pr_{x \sim \mathcal{P}_z}(\hat{p}(z|f(x)) \leq \gamma \hat{p}(z'|f(x)))$, and by definition of the linear softmax classifier, we have that

$$\begin{aligned} L_{\gamma, f}(z) &= \Pr_{x \sim \mathcal{P}_z} \left(\frac{\exp(f(x)^\top W_z)}{\exp(f(x)^\top W_z) + \exp(f(x)^\top W_{z'})} \leq \gamma \frac{\exp(f(x)^\top W_{z'})}{\exp(f(x)^\top W_z) + \exp(f(x)^\top W_{z'})} \right) \\ &= \Pr_{x \sim \mathcal{P}_z} (f(x)^\top (W_z - W_{z'}) \leq \log \gamma). \end{aligned} \quad (5)$$

To lower bound this quantity, we focus on upper bounding $f(x)^\top (W_z - W_{z'})$. We can bound $f_{SC}(x)^\top (W_z - W_{z'}) \leq \|W_z - W_{z'}\| \leq \|\mathbb{E}_{x \sim \mathcal{P}_z} [f_{SC}(x)] - \mathbb{E}_{x' \sim \mathcal{P}_{z'}} [f_{SC}(x')]\| + \xi_z + \xi_{z'}$, where $\xi_z = \left\| \frac{1}{m_z} \sum_{x \in \mathcal{D}_{s,z}} f_{SC}(x) - \mathbb{E}_{x \sim \mathcal{P}_z} [f_{SC}(x)] \right\|$ can be bounded via standard concentration inequalities and $\xi_{z'}$ is similarly constructed.

Because SupCon yields collapsed training embeddings within any class, we know that $f_{SC}(x) = f_{SC}(x')$ for $x, x' \in \mathcal{D}$ where $h_s(x) = z$ and $h_s(x') = z'$. Therefore, it holds that

$$\begin{aligned} &\|\mathbb{E}_{x \sim \mathcal{P}_z} [f_{SC}(x)] - \mathbb{E}_{x' \sim \mathcal{P}_{z'}} [f_{SC}(x')]\| \\ &= \left\| \mathbb{E}_{x \sim \mathcal{P}_z} [f_{SC}(x)] - \frac{1}{n_z} \sum_{x \in \mathcal{D}_z} f_{SC}(x) + \frac{1}{n_{z'}} \sum_{x' \in \mathcal{D}_{z'}} f_{SC}(x') - \mathbb{E}_{x' \sim \mathcal{P}_{z'}} [f_{SC}(x')] \right\| \\ &\leq \left\| \mathbb{E}_{x \sim \mathcal{P}_z} [f_{SC}(x)] - \frac{1}{n_z} \sum_{x \in \mathcal{D}_z} f_{SC}(x) \right\| + \left\| \frac{1}{n_{z'}} \sum_{x' \in \mathcal{D}_{z'}} f_{SC}(x') - \mathbb{E}_{x' \sim \mathcal{P}_{z'}} [f_{SC}(x')] \right\| \\ &\leq \sup_{f \in \mathcal{F}} \left\| \mathbb{E}_{x \sim \mathcal{P}_z} [f(x)] - \frac{1}{n_z} \sum_{x \in \mathcal{D}_z} f(x) \right\| + \sup_{f \in \mathcal{F}} \left\| \frac{1}{n_{z'}} \sum_{x' \in \mathcal{D}_{z'}} f(x') - \mathbb{E}_{x' \sim \mathcal{P}_{z'}} [f(x')] \right\|. \end{aligned}$$

Define $\epsilon(z, \mathcal{D}, \mathcal{F}) = \sup_{f \in \mathcal{F}} \|\mathbb{E}_{x \sim \mathcal{P}_z} [f(x)] - \frac{1}{n_z} \sum_{x \in \mathcal{D}_z} f(x)\|$ and similarly $\epsilon(z', \mathcal{D}, \mathcal{F})$. Therefore, our loss in (5) satisfies

$$\begin{aligned} L_{\gamma, f_{SC}}(z) &\geq \Pr(\epsilon(z, \mathcal{D}, \mathcal{F}) + \epsilon(z', \mathcal{D}, \mathcal{F}) + \xi_z + \xi_{z'} \leq \log \gamma) \\ &\geq \Pr\left(\epsilon(z, \mathcal{D}, \mathcal{F}) \leq \frac{\log \gamma}{4}\right) \Pr\left(\epsilon(z', \mathcal{D}, \mathcal{F}) \leq \frac{\log \gamma}{4}\right) \Pr\left(\xi_z \leq \frac{\log \gamma}{4}\right) \Pr\left(\xi_{z'} \leq \frac{\log \gamma}{4}\right), \end{aligned} \quad (6)$$

where independence comes from the fact that data is i.i.d. sampled for each subclass and each \mathcal{D} and \mathcal{D}_s , and that we are taking the supremum over \mathcal{F} . Next, we bound $\epsilon(z, \mathcal{D}, \mathcal{F})$. Since $\|f(x)\| \leq 1$, we have that by Lemma 5 that with probability $1 - \delta$,

$$\epsilon(z, \mathcal{D}, \mathcal{F}) \leq 2\mathfrak{R}_{n_z}(\mathcal{F}) + d \sqrt{\frac{2 \log(d/\delta)}{n_z}}.$$

Setting $\epsilon := 2\mathfrak{R}_{n_z}(\mathcal{F}) + d \sqrt{\frac{2 \log(d/\delta)}{n_z}}$, we can write $\delta = d \exp\left(-\frac{n_z}{2d^2}(\epsilon - 2\mathfrak{R}_{n_z}(\mathcal{F}))^2\right)$. Therefore, for $\log \gamma \geq 8\mathfrak{R}_{n_z}(\mathcal{F})$, we have that

$$\Pr\left(\epsilon(z, \mathcal{D}, \mathcal{F}) \leq \frac{\log \gamma}{4}\right) \geq 1 - d \exp\left(-\frac{n_z}{32d^2}(\log \gamma - 8\mathfrak{R}_{n_z}(\mathcal{F}))^2\right). \quad (7)$$

Next, we bound ξ_z . We can write

$$\left\| \frac{1}{m_z} \sum_{x \in \mathcal{D}_{s,z}} f_{SC}(x) - \mathbb{E}_{x \sim \mathcal{P}_z} [f_{SC}(x)] \right\| = \left(\sum_{j=1}^d \left(\frac{1}{m_z} \sum_{x \in \mathcal{D}_{s,z}} f_{SC}(x)[j] - \mathbb{E}_{x \sim \mathcal{P}_z} [f_{SC}(x)[j]] \right)^2 \right)^{1/2},$$

where $f_{SC}(x)[j]$ is the j th element of $f_{SC}(x)$. Using Hoeffding's inequality, we have that $\Pr\left(\frac{1}{m_z} \sum_{x \in \mathcal{D}_{s,z}} f_{SC}(x)[j] - \mathbb{E}_{x \sim \mathcal{P}_z} [f_{SC}(x)[j]] \geq \epsilon\right) \leq 2 \exp(-\frac{m_z \epsilon^2}{2})$, and therefore

$$\begin{aligned} & \Pr \left(\sum_{j=1}^d \left(\frac{1}{m_z} \sum_{x \in \mathcal{D}_{s,z}} f_{SC}(x)[j] - \mathbb{E}_{x \sim \mathcal{P}_z} [f_{SC}(x)[j]] \right)^2 \leq d\epsilon \right) \\ & \geq \Pr \left(\bigcap_{j=1}^d \left(\frac{1}{m_z} \sum_{x \in \mathcal{D}_{s,z}} f_{SC}(x)[j] - \mathbb{E}_{x \sim \mathcal{P}_z} [f_{SC}(x)[j]] \right)^2 \leq \epsilon \right) \\ & \geq \left(1 - 2 \exp \left(-\frac{m_z \epsilon}{2} \right) \right)^d \geq 1 - 2d \exp \left(-\frac{m_z \epsilon}{2} \right). \end{aligned}$$

That is, $\Pr(\xi_z \leq \sqrt{d\epsilon}) \geq 1 - 2d \exp \left(-\frac{m_z \epsilon}{2} \right)$.

Setting $\frac{\log \gamma}{4} = \sqrt{d\epsilon}$ gives us $\Pr(\xi_z \leq \frac{\log \gamma}{4}) \geq 1 - 2d \exp(-\frac{m_z \cdot \log^2 \gamma / 16d}{2}) = 1 - 2d \exp(-\frac{m_z \cdot \log^2 \gamma}{32d})$.

We put this expression and (7) back into (6) and use the fact that $(1 - \delta_1)(1 - \delta_2) \geq 1 - \delta_1 - \delta_2$ for any $\delta_1, \delta_2 > 0$. Therefore, we have for SupCon,

$$\begin{aligned} L_{\gamma, f_{SC}}(z) & \geq 1 - d \exp \left(-\frac{n_z}{32d^2} (\log \gamma - 8\mathfrak{R}_{n_z}(\mathcal{F}))^2 \right) - d \exp \left(-\frac{n_{z'}}{32d^2} (\log \gamma - 8\mathfrak{R}_{n_{z'}}(\mathcal{F}))^2 \right) \\ & \quad - 2d \exp \left(-\frac{m_z \log^2 \gamma}{32d} \right) - 2d \exp \left(-\frac{m_{z'} \log^2 \gamma}{32d} \right) \\ & \geq 1 - d \exp \left(-\frac{n_z}{32d^2} (\log \gamma - 8\mathfrak{R}_{n_z}(\mathcal{F}))^2 \right) - d \exp \left(-\frac{n_{z'}}{32d^2} (\log \gamma - 8\mathfrak{R}_{n_{z'}}(\mathcal{F}))^2 \right) \\ & \quad - 4d \exp \left(-\frac{(m_z \wedge m_{z'}) \log^2 \gamma}{32d} \right) \\ & = 1 - \delta(n_z, \mathcal{F}, \gamma) - \delta(n_{z'}, \mathcal{F}, \gamma) - \xi(m_z \wedge m_{z'}, \gamma). \end{aligned}$$

□

Proposition 1 (Individual losses). $L_{\text{align}}(f)$ and $L_{\text{aug}}(f)$ are minimized when $f(x) = f(x^+)$ and $f(x) = f(a(x))$ almost surely, respectively. $L_{\text{diff}}(\mu)$ is minimized when $\mu = \delta_v$. $L_{\text{same}}(\mu)$ is minimized when $\mu = \sigma_{d-1}$.

Proof. For both $L_{\text{align}}(f)$ and $L_{\text{aug}}(f)$, the minimum value of the expression is 0, which is obtained when $f(x) = f(x^+)$ and $f(x) = f(x^a)$ almost surely, respectively.

For $L_{\text{diff}}(f)$, we can equivalently consider minimizing $\mathbb{E}_{x, x'} [\exp(-\|f(x) - f(x')\|^2 / 2\tau)]$. Note that $\max_{f(x), f(x') \in \mathcal{S}^{d-1}} \|f(x) - f(x')\| = 2$, and so $\inf \mathbb{E}_{x, x'} [\exp(-\|f(x) - f(x')\|^2 / 2\tau)] = \exp(-2/\tau)$. For $\mu = \delta_v$,

$$\begin{aligned} \mathbb{E}_{x, x'} [\exp(-\|f(x) - f(x')\|^2 / 2\tau)] & = \frac{1}{2} \mathbb{E}_{h(x)=0, h(x')=1} [\exp(-\|v_0 - v_1\|^2 / 2\tau)] \\ & \quad + \frac{1}{2} \mathbb{E}_{h(x)=1, h(x')=0} [\exp(-\|v_1 - v_0\|^2 / 2\tau)] \\ & = \exp(-\|v_0 - v_1\|^2 / 2\tau) = \exp(-2/\tau) \end{aligned} \tag{8}$$

The first equality follows from class balance, and the third equality follows from the definition of the regular simplex. Therefore, $\mu = \delta_v$ minimizes $L_{\text{diff}}(f)$.

For $L_{\text{same}}(f)$, we can equivalently consider minimizing $\mathbb{E}_{x,x^+} [\exp(-\|(f(x) - f(x^+))\|^2/2\tau)]$. We can write this as

$$\begin{aligned} \mathbb{E}_{x,x^+} [\exp(-\|(f(x) - f(x^+))\|^2/2\tau)] &= \frac{1}{2} \mathbb{E}_{h(x)=h(x^+)=0} [\exp(-\|(f(x) - f(x^+))\|^2/2\tau)] \\ &\quad + \frac{1}{2} \mathbb{E}_{h(x)=h(x^+)=1} [\exp(-\|(f(x) - f(x^+))\|^2/2\tau)] \end{aligned} \quad (9)$$

Using the infinite encoder assumption, we can equivalently consider the following minimization problem over the hypersphere, where $u, u' \in \mathcal{S}^{d-1}$:

$$\text{minimize}_{\mu_0, \mu_1} \frac{1}{2} \int \int \exp(-\|u - u'\|^2/2\tau) d\mu_0(u) d\mu_0(u') + \frac{1}{2} \int \int \exp(-\|u - u'\|^2/2\tau) d\mu_1(u) d\mu_1(u') \quad (10)$$

Each of these integrals can be minimized individually, and the problem becomes equivalent to minimizing the Gaussian $\frac{1}{2\tau}$ -energy. Using Proposition 4.4.1 and Theorem 6.2.1 of [3], the optimal solution is $\mu_0 = \mu_1 = \sigma_{d-1}$, the normalized surface area measure. Therefore, $\boldsymbol{\mu} = \boldsymbol{\sigma}_{d-1}$. \square

Theorem 2. Let $c_{\tau,d} = \frac{2 + \frac{1}{\tau} - \sqrt{\frac{1}{\tau}(-2 + \frac{1}{\tau}) - 2 \log W_{1/2\tau}(\mathcal{S}^{d-1})}}{3}$, where $W_{1/2\tau}(\mathcal{S}^{d-1})$ is the Wiener constant of the Gaussian $\frac{1}{2\tau}$ -energy on \mathcal{S}^{d-1} , which is defined as

$$W_{1/2\tau}(\mathcal{S}^{d-1}) = \frac{2^{d-2} \Gamma(d/2)}{\sqrt{\pi} \Gamma((d-1)/2)} \int_0^1 \exp\left(-\frac{2u}{\tau}\right) (u(1-u))^{(d-3)/2} du,$$

where the Gamma function is $\Gamma(z) = \int_0^\infty x^{z-1} e^{-x} dx$ for $z > 0$. Then, when $\alpha \in (2/3, c_{\tau,d})$, $\theta^* = \arcsin \sqrt{\frac{\tau}{2} \log \frac{3\alpha-1}{3-3\alpha}}$ minimizes $L_{\text{spread}}(\boldsymbol{\mu}_\theta, \alpha)$ and satisfies $L_{\text{spread}}(\boldsymbol{\mu}_{\theta^*}, \alpha) \leq \min_{\boldsymbol{\mu} \in \{\boldsymbol{\delta}_v, \boldsymbol{\sigma}_{d-1}\}} L_{\text{spread}}(\boldsymbol{\mu}, \alpha)$.

Proof. Because the augmentations only play a role in $L_{\text{aug}}(f)$, the condition that $f(x) = f(x^a)$ a.s. is compatible with any of the other three losses in Proposition 1. Therefore, we focus on analyzing the combined weighted loss $(1-\alpha)L_{\text{align}}(f) + (1-\alpha)L_{\text{diff}}(f) + \alpha L_{\text{same}}(f)$. We use the fact that $K = 2$ for our analysis to simplify this loss:

$$\begin{aligned} L(\boldsymbol{\mu}, \alpha) &= (1-\alpha) \log \mathbb{E}_{h(x)=0, h(x^-)=1} \left[\exp\left(-\frac{1}{2\tau} \|f(x) - f(x^-)\|^2\right) \right] \\ &\quad + \alpha \log \mathbb{E}_{h(x)=h(x^+)=0} \left[\exp\left(-\frac{1}{2\tau} \|f(x) - f(x^+)\|^2\right) \right] + (1-\alpha) \mathbb{E}_{h(x)=h(x^+)=0} \left[\frac{1}{2\tau} \|f(x) - f(x^+)\|^2 \right]. \end{aligned}$$

We first define a new distribution $\boldsymbol{\mu}_\theta = \{\mu_{0,\theta}, \mu_{1,\theta}\}$ for $\theta \in (0, \pi/2]$ that involves ‘‘splitting’’ $\boldsymbol{\delta}_v$. Without loss of generality, suppose that $v_0 = e_1$ and $v_1 = -e_1$, where $e_1 \in \mathbb{R}^d$ is a standard basis vector $[1, 0, \dots, 0]$ where all but the first two elements are always 0. For v_0 , we consider the vectors $v_{0,\theta} = [\cos \theta, \sin \theta, \dots, 0]$ and $v_{0,-\theta} = [\cos \theta, -\sin \theta, \dots, 0]$. For v_1 , we consider the vectors $v_{1,\theta} = [-\cos \theta, -\sin \theta, \dots, 0]$ and $v_{1,-\theta} = [-\cos \theta, \sin \theta, \dots, 0]$. Now, we are able to define $\boldsymbol{\mu}_\theta$. Let $\mu_{0,\theta} = \frac{1}{2} \delta_{v_{0,\theta}} + \frac{1}{2} \delta_{v_{0,-\theta}}$ and let $\mu_{1,\theta} = \frac{1}{2} \delta_{v_{1,\theta}} + \frac{1}{2} \delta_{v_{1,-\theta}}$. That is, each class-conditional measure is a mixture on two points separated by θ .

The first step is to show that for some range of α , $\min_\theta L(\boldsymbol{\mu}_\theta, \alpha) < L(\boldsymbol{\delta}_v, \alpha)$. We have that

$$L(\boldsymbol{\delta}_v, \alpha) = (1-\alpha) \log \exp\left(-\frac{4}{2\tau}\right) + \alpha \log \exp(0) + (1-\alpha) \cdot 0 = -\frac{2(1-\alpha)}{\tau}. \quad (11)$$

and

$$\begin{aligned} L(\boldsymbol{\mu}_\theta, \alpha) &= (1-\alpha) \log \left(\frac{1}{2} \exp\left(-\frac{4}{2\tau}\right) + \frac{1}{2} \exp\left(-\frac{4 \cos^2 \theta}{2\tau}\right) \right) + \alpha \log \left(\frac{1}{2} + \frac{1}{2} \exp\left(-\frac{4 \sin^2 \theta}{2\tau}\right) \right) \\ &\quad + \frac{1-\alpha}{2\tau} \cdot \frac{1}{2} (4 \sin^2 \theta) \\ &= -\log 2 - \frac{2(1-\alpha)}{\tau} + (1-\alpha) \log \left(1 + \exp\left(\frac{2 \sin^2 \theta}{\tau}\right) \right) + \alpha \log \left(1 + \exp\left(-\frac{2 \sin^2 \theta}{\tau}\right) \right) \\ &\quad + \frac{(1-\alpha) \sin^2 \theta}{\tau}. \end{aligned} \quad (12)$$

We now compute the derivative $\frac{\partial L(\boldsymbol{\mu}_\theta, \alpha)}{\partial \theta}$ to find local minima:

$$\begin{aligned} \frac{\partial L(\boldsymbol{\mu}_\theta, \alpha)}{\partial \theta} &= (1 - \alpha) \frac{\exp\left(\frac{2 \sin^2 \theta}{\tau}\right) \cdot \frac{4 \sin \theta \cos \theta}{\tau}}{1 + \exp\left(\frac{2 \sin^2 \theta}{\tau}\right)} + \alpha \frac{\exp\left(-\frac{2 \sin^2 \theta}{\tau}\right) \cdot \frac{-4 \sin \theta \cos \theta}{\tau}}{1 + \exp\left(-\frac{2 \sin^2 \theta}{\tau}\right)} + \frac{(1 - \alpha) 4 \sin \theta \cos \theta}{\tau} \\ &= \frac{4 \sin \theta \cos \theta}{\tau} \left((1 - \alpha) \frac{\exp(2 \sin^2 \theta / \tau)}{1 + \exp(2 \sin^2 \theta / \tau)} - \alpha \frac{\exp(-2 \sin^2 \theta / \tau)}{1 + \exp(-2 \sin^2 \theta / \tau)} + \frac{1 - \alpha}{2} \right). \end{aligned}$$

Note that $\sin \theta$ and $\cos \theta$ are positive for $\theta \in (0, \pi/2]$. Next, for notational simplicity let $x = \frac{2 \sin^2 \theta}{\tau}$. Then, we can equivalently evaluate

$$\begin{aligned} (1 - \alpha) \frac{e^x}{1 + e^x} - \alpha \frac{e^{-x}}{1 + e^{-x}} + \frac{1 - \alpha}{2} &= (1 - \alpha) \frac{e^x}{1 + e^x} - \alpha \frac{1}{1 + e^x} + \frac{1 - \alpha}{2} \\ &= \frac{e^x - \alpha(1 + e^x)}{1 + e^x} + \frac{1 - \alpha}{2} \\ &= \frac{e^x}{1 + e^x} + \frac{1}{2} - \frac{3\alpha}{2}. \end{aligned}$$

Setting this equal to 0, we get that $\alpha = \frac{3e^x + 1}{3e^x + 3}$ and $x = \log \frac{3\alpha - 1}{3 - 3\alpha}$. Since $x \in (0, 2/\tau]$, we have that if $\alpha \in \left(\frac{2}{3}, \frac{3 \exp(2/\tau) + 1}{3 \exp(2/\tau) + 3}\right)$, there exists a local optima over $\theta \in (0, \pi/2]$.

Moreover, we observe that when $\alpha \leq 2/3$, we have that $\frac{e^x}{1 + e^x} + \frac{1}{2} - \frac{3\alpha}{2} \geq \frac{e^x}{1 + e^x} - \frac{1}{2} \geq 0$, which means that $L(\boldsymbol{\mu}_\theta, \alpha)$ increases in θ for $\alpha \leq 2/3$. Therefore, when $\alpha \leq 2/3$, class collapse is *always better* no matter the angle, and $L(\boldsymbol{\delta}_v, \alpha) \leq \min_\theta L(\boldsymbol{\mu}_\theta, \alpha)$.

Next, we consider when $\alpha \geq \frac{3 \exp(2/\tau) + 1}{3 \exp(2/\tau) + 3}$. In this case, $\frac{e^x}{1 + e^x} + \frac{1}{2} - \frac{3\alpha}{2} < 0$, so $L(\boldsymbol{\mu}_\theta, \alpha)$ is decreasing in θ . This means that any nonzero θ in this setting is going to result in a smaller loss than the class-collapsed loss.

Lastly, we consider the intermediate case of $\alpha \in \left(\frac{2}{3}, \frac{3 \exp(2/\tau) + 1}{3 \exp(2/\tau) + 3}\right)$. Plugging back in $x = \log \frac{3\alpha - 1}{3 - 3\alpha}$ back into $L(\boldsymbol{\mu}_\theta, \alpha)$ in (12), we have

$$\begin{aligned} L(\boldsymbol{\mu}_\theta, \alpha) &= -\log 2 - \frac{2(1 - \alpha)}{\tau} + (1 - \alpha) \log \left(1 + \frac{3\alpha - 1}{3 - 3\alpha}\right) + \alpha \log \left(1 + \frac{3 - 3\alpha}{3\alpha - 1}\right) + \frac{1 - \alpha}{2} \cdot \log \frac{3\alpha - 1}{3 - 3\alpha} \\ &= -\log 2 - \frac{2(1 - \alpha)}{\tau} + (1 - \alpha) \log \frac{2}{3 - 3\alpha} + \alpha \log \frac{2}{3\alpha - 1} + \frac{1 - \alpha}{2} \log(3\alpha - 1) - \frac{1 - \alpha}{2} \log(3 - 3\alpha) \\ &= -\frac{2(1 - \alpha)}{\tau} - \frac{3 - 3\alpha}{2} \log(3 - 3\alpha) - \frac{3\alpha - 1}{2} \log(3\alpha - 1). \end{aligned} \tag{13}$$

Note that $(3 - 3\alpha) \log(3 - 3\alpha) + (3\alpha - 1) \log(3\alpha - 1)$ equals 0 at $\alpha = 2/3$ and is increasing in α . Therefore, we have that $-\frac{2(1 - \alpha)}{\tau} - \frac{3 - 3\alpha}{2} \log(3 - 3\alpha) - \frac{3\alpha - 1}{2} \log(3\alpha - 1) \leq -\frac{2(1 - \alpha)}{\tau} = L(\boldsymbol{\delta}_v, \alpha)$. Therefore, for $\alpha \in \left(\frac{2}{3}, \frac{3 \exp(2/\tau) + 1}{3 \exp(2/\tau) + 3}\right)$, the optimal θ^* satisfies $L(\boldsymbol{\mu}_\theta, \alpha) \leq L(\boldsymbol{\delta}_v, \alpha)$. In particular, solving $\frac{2 \sin^2 \theta^*}{\tau} = \log \frac{3\alpha - 1}{3 - 3\alpha}$ gives us $\theta^* = \arcsin \sqrt{\frac{\tau}{2} \log \frac{3\alpha - 1}{3 - 3\alpha}}$.

Therefore, our analysis in these three ranges of α suggest that the optimal embedding geometry is *not collapsed* when $\alpha \geq \frac{2}{3}$.

Next, we want to understand when the optimal embedding geometry is not $\boldsymbol{\sigma}_{d-1}$. A sufficient condition for this is to show that there exists an $\alpha \geq \frac{2}{3}$ where $\min_\theta L(\boldsymbol{\mu}_\theta, \alpha) \leq L(\boldsymbol{\sigma}_{d-1}, \alpha)$. We first compute an upper bound on $\min_\theta L(\boldsymbol{\mu}_\theta, \alpha)$ for $\alpha > \frac{2}{3}$. Recall that our loss from (13) can be written as

$$L(\boldsymbol{\mu}_\theta, \alpha) = -\frac{2(1 - \alpha)}{\tau} - \log 2 - \frac{3 - 3\alpha}{2} \log \left(\frac{3 - 3\alpha}{2}\right) - \frac{3\alpha - 1}{2} \log \left(\frac{3\alpha - 1}{2}\right). \tag{14}$$

For ease of notation, let $x = \frac{3 - 3\alpha}{2} \in (0, 1)$. We show that $f(x) = x \log x + (1 - x) \log(1 - x)$ can be lower bounded quadratically. Performing a Taylor expansion at $x = 0.5$, we have that $x \log x + (1 - x) \log(1 - x) \approx$

$-\log 2 + 2(x - 1/2)^2$. We claim that $x \log x + (1 - x) \log(1 - x) \geq -\log 2 + 2(x - 1/2)^2$. Note that the two sides are equal when $x = 1/2$, so proving this inequality is equivalent to showing that $f'(x) \geq 4(x - 1/2)$ for $x \geq 1/2$ and $f'(x) < 4(x - 1/2)$ for $x < 1/2$. $f'(x) = \log \frac{x}{1-x}$ is equal to $4(x - 1/2)$ at $x = 1/2$, so we want to show that $f''(x) \geq 4$ for all x . $f''(x) = \frac{1}{x(1-x)}$ satisfies this inequality. Therefore, (14) becomes

$$L(\boldsymbol{\mu}_\theta, \alpha) \leq -\frac{2(1-\alpha)}{\tau} - 2\left(1 - \frac{3\alpha}{2}\right)^2.$$

Next, we compute $L(\boldsymbol{\sigma}_{d-1}, \alpha)$. Define the Gaussian $\frac{1}{2\tau}$ -energy of σ_{d-1} on \mathcal{S}^{d-1} as

$$I_{1/2\tau}[\sigma_{d-1}] = \int_{\mathcal{S}^{d-1}} \int_{\mathcal{S}^{d-1}} \exp\left(-\frac{1}{2\tau}\|u - u'\|^2\right) d\sigma_{d-1}(u) d\sigma_{d-1}(u'). \quad (15)$$

Then, we have that

$$L(\boldsymbol{\sigma}_{d-1}, \alpha) = (1 - \alpha) \log I_{1/2\tau}[\sigma_{d-1}] + \alpha \log I_{1/2\tau}[\sigma_{d-1}] - \frac{1 - \alpha}{2\tau} \int \int -\|u - u'\|^2 d\sigma_{d-1}(u) d\sigma_{d-1}(u') \quad (16)$$

From Theorem 4.6.5 of Borodachov et al. [3], any measure μ that has mass centered at the origin, i.e. $\int u d\mu(u) = 0$, minimizes the energy $I_{-2}[\mu] = \int \int -\|u - u'\|^2 d\mu(u) d\mu(u')$. Therefore, $\int \int -\|u - u'\|^2 d\sigma_{d-1}(u) d\sigma_{d-1}(u')$ is equivalent to the energy $I_{-2}[\frac{1}{2}\delta_{v_0} + \frac{1}{2}\delta_{v_1}] = -\frac{1}{2}(2^2) = -2$, since a measure on two points with probability 1/2 each has mass centered at the origin. Plugging this back into $L(\boldsymbol{\sigma}_{d-1}, \alpha)$ in (16), we have

$$L(\boldsymbol{\sigma}_{d-1}, \alpha) = \log I_{1/2\tau}[\sigma_{d-1}] + \frac{1 - \alpha}{\tau}.$$

From Proposition 4.4.1 and Theorem 6.2.1 of Borodachov et al. [3], σ_{d-1} is the unique equilibrium measure for the Gaussian $\frac{1}{2\tau}$ kernel on \mathcal{S}^{d-1} , and as a result $I_{1/2\tau}[\sigma_{d-1}]$ is equal to the Wiener constant $W_{1/2\tau}(\mathcal{S}^{d-1})$, which has the value

$$W_{1/2\tau}(\mathcal{S}^{d-1}) = \frac{2^{d-2}\Gamma(d/2)}{\sqrt{\pi}\Gamma((d-1)/2)} \int_0^1 \exp\left(-\frac{2u}{\tau}\right) (u(1-u))^{(d-3)/2} du, \quad (17)$$

where the Gamma function is $\Gamma(z) = \int_0^\infty x^{z-1} e^{-x} dx$ for $z > 0$.

Therefore, to prove that there exists a $\boldsymbol{\mu}_\theta$ that has lower loss than $\boldsymbol{\sigma}_{d-1}$, we must find $\alpha > 2/3$ that satisfies

$$2\left(1 - \frac{3\alpha}{2}\right)^2 + \frac{3(1-\alpha)}{\tau} + \log W_{1/2\tau}(\mathcal{S}^{d-1}) \geq 0.$$

This expression is quadratic in α , and we solve it to get that $c(\tau, d) \leq \frac{2 + \frac{1}{\tau} - \sqrt{\frac{1}{\tau}(-2 + \frac{1}{\tau}) - 2 \log W_{1/2\tau}(\mathcal{S}^{d-1})}}{3}$. \square

C.2 Proofs for Section 4

Proposition 2. *Let \mathcal{F} be the set of infinite encoders. Then L_{spread} is invariant on class-fixing permutations under \mathcal{F} .*

Proof. We know that any $f^\pi \in \mathcal{F}$ can satisfy $f^\pi(x_i) = f(x_{\pi(i)})$, since the infinite encoder assumption means that f^π can be arbitrarily fit to any data. Therefore, we only need to show that L_{spread} does not change when f^π , which permutes within classes, is used instead of f .

For a given batch B and f , L_{spread} is constructed as defined in Section 2.2. The numerator of L_{sup} can be written as $\frac{1}{|B|} \frac{1}{|P(i, B)|} \sum_{i=1}^{|B|} \sum_{x^+ \in P(i, B)} \log \sigma_f(x_i, x^+)$. This is a summation over the representations of all positive pairs in the batch. Therefore, a permutation π within each class that changes the assignments to the representations will not change the value of this quantity, and $\frac{1}{|B|} \frac{1}{|P(i, B)|} \sum_{i=1}^{|B|} \sum_{x^+ \in P(i, B)} \log \sigma_{f^\pi}(x_i, x^+) = \frac{1}{|B|} \frac{1}{|P(i, B)|} \sum_{i=1}^{|B|} \sum_{x^+ \in P(i, B)} \log \sigma_f(x_i, x^+)$.

Next, the denominator of L_{sup} can be written as $\frac{1}{|P(i,B)|} \sum_{i=1}^{|B|} \sum_{x^+ \in P(i,B)} \log \left(\sigma_f(x_i, x^+) + \sum_{x^- \in N(i,B)} \sigma_f(x_i, x^-) \right)$. Every single positive pair and negative pair is included in this expression, so this quantity is class-fixing permutation invariant.

The numerator of L_{cNCE} is $\frac{1}{|B|} \sum_{i=1}^{|B|} \log \sigma_f(x_i, a(x_i))$. Since an augmentation of x_i is a function of x_i and is disjoint from augmentations of other points, this quantity is class-fixing permutation invariant.

Lastly, the denominator of L_{cNCE} is $\frac{1}{|B|} \sum_{i=1}^{|B|} \log \left(\sum_{x^+ \in P(i,B)} \sigma_f(x_i, x^+) \right)$. From the same logic as the numerator of L_{sup} , any permutation within the class will still allow each x_i to be compared with all other points in x_i 's class, hence being class-fixing permutation invariant.

Therefore, under the infinite encoder assumption where all f^π are valid, L_{spread} is permutation invariant. \square

Theorem 3. Denote $r_f(z, z') = c^2 \delta_f(z, z')^2 - |\text{Var}_f[z] - \text{Var}_f[z']|$. With probability $1 - \delta$, the coarse-to-fine error is at most

$$L_{\gamma, f}(z) \leq \frac{\sigma_f(z)}{\sqrt{r_f(z, z') - 2 \log \gamma}} + \mathcal{O}\left(\left(\frac{d \log(d/\delta)}{m_z \wedge m_{z'}}\right)^{1/4}\right).$$

under the boundary condition that $r_f(z, z') - 2 \log \gamma \geq 16 \sqrt{\frac{2d \log(8d/\delta)}{m_z \wedge m_{z'}}} + \frac{2d \log(8d/\delta)}{m_z}$.

Proof. From (5), our loss function can be written as $L_{\gamma, f}(z) = \Pr_{x \sim \mathcal{P}_z} (f(x)^\top (W_z - W_{z'}) \leq \log \gamma)$. Note that $\|f(x) - W_z\|^2 = \|f(x)\|^2 + \|W_z\|^2 - 2f(x)^\top W_z = 1 + \|W_z\|^2 - 2f(x)^\top W_z$, which means that $f(x)^\top W_z = \frac{1}{2} (1 + \|W_z\|^2 - \|f(x) - W_z\|^2)$. We can thus write our loss as

$$\begin{aligned} L_{\gamma, f}(z) &= \Pr_{x \sim \mathcal{P}_z} (f(x)^\top (W_z - W_{z'}) \leq \log \gamma) \\ &= \Pr_{x \sim \mathcal{P}_z} (\|f(x) - W_z\| \geq (\|f(x) - W_{z'}\|^2 - 2 \log \gamma + \|W_z\|^2 - \|W_{z'}\|^2)^{1/2}). \end{aligned} \quad (18)$$

We bound terms in this probability individually. First, we can write

$$\|f(x) - W_z\| \leq \|f(x) - \mathbb{E}_{x \sim \mathcal{P}_z} [f(x)]\| + \xi_z, \quad (19)$$

where ξ_z again is constructed as $\xi_z = \|W_z - \mathbb{E}_{x \sim \mathcal{P}_z} [f(x)]\| = \left\| \frac{1}{m_z} \sum_{x \in \mathcal{D}_{s,z}} f_{SC}(x) - \mathbb{E}_{x \sim \mathcal{P}_z} [f_{SC}(x)] \right\|$.

Next, by the reverse triangle inequality we can write

$$\begin{aligned} \|f(x) - W_{z'}\|^2 &\geq \left| \|f(x) - \mathbb{E}_{x \sim \mathcal{P}_{z'}} [f(x)]\| - \|\mathbb{E}_{x \sim \mathcal{P}_{z'}} [f(x)] - W_{z'}\| \right|^2 \\ &\geq \|f(x) - \mathbb{E}_{x \sim \mathcal{P}_{z'}} [f(x)]\|^2 - 2\|f(x) - \mathbb{E}_{x \sim \mathcal{P}_{z'}} [f(x)]\| \xi_{z'} \\ &\geq \|f(x) - \mathbb{E}_{x \sim \mathcal{P}_{z'}} [f(x)]\|^2 - 4\xi_{z'} \\ &\geq c^2 \cdot \mathbb{E}_{x \sim \mathcal{P}_z, x' \sim \mathcal{P}_{z'}} [\|f(x) - f(x')\|^2] - 4\xi_{z'}. \end{aligned} \quad (20)$$

Note the following decomposition by Jensen's inequality:

$$\begin{aligned} s_f(y) &= \mathbb{E}_{h(x)=y} [\|f(x) - \mathbb{E}_{h(x)=y} [f(x)]\|] \leq p(z|y)^2 \mathbb{E}_{x \sim \mathcal{P}_z} [\|f(x) - \mathbb{E}_{x \sim \mathcal{P}_z} [f(x)]\|] \\ &\quad + p(z'|y)^2 \mathbb{E}_{x \sim \mathcal{P}_{z'}} [\|f(x) - \mathbb{E}_{x \sim \mathcal{P}_{z'}} [f(x)]\|] + p(z|y)p(z'|y) \mathbb{E}_{x \sim \mathcal{P}_z} [\|f(x) - \mathbb{E}_{x' \sim \mathcal{P}_{z'}} [f(x')] \|] \\ &\quad + p(z|y)p(z'|y) \mathbb{E}_{x \sim \mathcal{P}_{z'}} [\|f(x) - \mathbb{E}_{x' \sim \mathcal{P}_z} [f(x')] \|] \\ &\leq p(z|y)^2 \sigma_f(z) + p(z'|y)^2 \sigma_f(z') + 2p(z|y)p(z'|y) \mathbb{E}_{x \sim \mathcal{P}_z, x' \sim \mathcal{P}_{z'}} [\|f(x) - f(x')\|], \end{aligned}$$

and thus, $\mathbb{E}_{x \sim \mathcal{P}_z, x' \sim \mathcal{P}_{z'}} [\|f(x) - f(x')\|] \geq \delta_f(z, z') = \frac{1}{p(z|y)p(z'|y)} \cdot (s_f(y) - p(z|y)^2 \sigma_f(z) - p(z'|y)^2 \sigma_f(z'))$.

Then, (20) becomes

$$\|f(x) - W_{z'}\|^2 \geq c^2 \cdot \delta_f(z, z')^2 - 4\xi_{z'}. \quad (21)$$

Finally, we bound $\|W_z\|^2 - \|W_{z'}\|^2$. Recall that $\|W_z\|^2 = \left\| \frac{1}{m_z} \sum_{x \in \mathcal{D}_{s,z}} f(x) \right\|^2$. We can write the empirical variance $\frac{1}{m_z} \sum_{x \in \mathcal{D}_{s,z}} \|f(x) - \frac{1}{m_z} \sum_{x \in \mathcal{D}_{s,z}} f(x)\|^2$ as $1 + \|W_z\|^2 - \frac{1}{m_z} \sum_{x \in \mathcal{D}_{s,z}} f(x)^\top \frac{2}{m_z} \sum_{x \in \mathcal{D}_{s,z}} f(x) = 1 - \|W_z\|^2$, and therefore,

$$\begin{aligned} \left| \|W_z\|^2 - \|W_{z'}\|^2 \right| &\leq \left| \frac{1}{m_z} \sum_{x \in \mathcal{D}_{s,z}} \|f(x) - \frac{1}{m_z} \sum_{x \in \mathcal{D}_{s,z}} f(x)\|^2 - \frac{1}{m_{z'}} \sum_{x \in \mathcal{D}_{s,z'}} \|f(x) - \frac{1}{m_{z'}} \sum_{x \in \mathcal{D}_{s,z'}} f(x)\|^2 \right| \\ &\leq \left| \frac{1}{m_{z'}} \sum_{x \in \mathcal{D}_{s,z'}} \left\| f(x) - \frac{1}{m_{z'}} \sum_{x \in \mathcal{D}_{s,z'}} f(x) \right\|^2 - \mathbb{E}_{x \sim \mathcal{P}_{z'}} [\|f(x) - \mathbb{E}_{x \sim \mathcal{P}_{z'}} [f(x)]\|^2] \right| \\ &\quad + \left| \frac{1}{m_z} \sum_{x \in \mathcal{D}_{s,z}} \left\| f(x) - \frac{1}{m_z} \sum_{x \in \mathcal{D}_{s,z}} f(x) \right\|^2 - \mathbb{E}_{x \sim \mathcal{P}_z} [\|f(x) - \mathbb{E}_{x \sim \mathcal{P}_z} [f(x)]\|^2] \right| \\ &\quad + |\text{Var}_f [z] - \text{Var}_f [z']|. \end{aligned} \quad (22)$$

where $\text{Var}_f [z] = \mathbb{E}_{x \sim \mathcal{P}_z} [\|f(x) - \mathbb{E}_{x \sim \mathcal{P}_z} [f(x)]\|^2]$, and $\text{Var}_f [z']$ is similarly defined. We decompose the first term in (22) and bound it by

$$\begin{aligned} &\left| \frac{1}{m_{z'}} \sum_{x \in \mathcal{D}_{s,z'}} \left\| f(x) - \frac{1}{m_{z'}} \sum_{x \in \mathcal{D}_{s,z'}} f(x) \right\|^2 - \frac{1}{m_{z'}} \sum_{x \in \mathcal{D}_{s,z'}} \|f(x) - \mathbb{E}_{x \sim \mathcal{P}_{z'}} [f(x)]\|^2 \right| \\ &+ \left| \frac{1}{m_{z'}} \sum_{x \in \mathcal{D}_{s,z'}} \|f(x) - \mathbb{E}_{x \sim \mathcal{P}_{z'}} [f(x)]\|^2 - \mathbb{E}_{x \sim \mathcal{P}_{z'}} [\|f(x) - \mathbb{E}_{x \sim \mathcal{P}_{z'}} [f(x)]\|^2] \right| \\ &= \frac{1}{m_{z'}} \sum_{x \in \mathcal{D}_{s,z'}} \left| \left\| f(x) - \frac{1}{m_{z'}} \sum_{x \in \mathcal{D}_{s,z'}} f(x) \right\|^2 - \|f(x) - \mathbb{E}_{x \sim \mathcal{P}_{z'}} [f(x)]\|^2 \right| + \zeta_{z'} \\ &\leq \frac{1}{m_{z'}} \sum_{x \in \mathcal{D}_{s,z'}} 4 \left| \left\| f(x) - \frac{1}{m_{z'}} \sum_{x \in \mathcal{D}_{s,z'}} f(x) \right\| - \|f(x) - \mathbb{E}_{x \sim \mathcal{P}_{z'}} [f(x)]\| \right| + \zeta_{z'} \\ &\leq \frac{1}{m_{z'}} \sum_{x \in \mathcal{D}_{s,z'}} 4 \left| \frac{1}{m_{z'}} \sum_{x \in \mathcal{D}_{s,z'}} f(x) - \mathbb{E}_{x \sim \mathcal{P}_{z'}} [f(x)] \right| + \zeta_{z'} \\ &\leq 4\xi_{z'} + \zeta_{z'}. \end{aligned}$$

where $\zeta_{z'} = \left| \frac{1}{m_{z'}} \sum_{x \in \mathcal{D}_{s,z'}} \|f(x) - \mathbb{E}_{x \sim \mathcal{P}_{z'}} [f(x)]\|^2 - \mathbb{E}_{x \sim \mathcal{P}_{z'}} [\|f(x) - \mathbb{E}_{x \sim \mathcal{P}_{z'}} [f(x)]\|^2] \right|$ can be bounded by standard concentration inequalities. Therefore, $\left| \|W_z\|^2 - \|W_{z'}\|^2 \right|$ is bounded by

$$\left| \|W_z\|^2 - \|W_{z'}\|^2 \right| \leq |\text{Var}_f [z] - \text{Var}_f [z']| + 4\xi_z + 4\xi_{z'} + \zeta_z + \zeta_{z'}. \quad (23)$$

Then, combining (19), (21), and (23), the loss in (18) becomes

$$L_{\gamma, f}(z) \leq \Pr_{x \sim \mathcal{P}_z} (\|f(x) - \mathbb{E}_{x \sim \mathcal{P}_z} [f(x)]\| \geq (r_f(z, z') - 8\xi_{z'} - 4\xi_z - \zeta_z - \zeta_{z'} - 2 \log \gamma)^{1/2} - \xi_z). \quad (24)$$

Next, we note that $\xi_z \leq \sqrt{\frac{2d \log(2d/\delta)}{m_z}}$ with probability at least $1 - \delta$. Applying Hoeffding's inequality on ζ_z gives us $\zeta_z \leq \sqrt{\frac{8 \log(2/\delta)}{m_z}}$ with probability at least $1 - \delta$. Applying a union bound, we have that with probability $1 - \delta$, (24)

satisfies

$$L_{\gamma, f}(z) \leq \Pr_{x \sim \mathcal{P}_z} \left(\left\| f(x) - \mathbb{E}_{x \sim \mathcal{P}_z} [f(x)] \right\| \geq \left(r_f(z, z') - 10 \sqrt{\frac{2d \log(8d/\delta)}{m_{z'}}} - 6 \sqrt{\frac{2d \log(8d/\delta)}{m_z}} - 2 \log \gamma \right)^{1/2} - \sqrt{\frac{2d \log(8d/\delta)}{m_z}} \right).$$

Finally, we can apply Markov's inequality under the condition that $r_f(z, z') - 2 \log \gamma \geq \frac{2d \log(8d/\delta)}{m_z} + 6 \sqrt{\frac{2d \log(8d/\delta)}{m_z}} + 10 \sqrt{\frac{2d \log(8d/\delta)}{m_{z'}}$, or equivalently $r_f(z, z') - 2 \log \gamma \geq \frac{2d \log(8d/\delta)}{m_z} + 16 \sqrt{\frac{2d \log(8d/\delta)}{m_z \wedge m_{z'}}$. With probability at least $1 - \delta$, our loss is bounded by

$$\begin{aligned} L_{\gamma, f}(z) &\leq \frac{\mathbb{E}_{x \sim \mathcal{P}_z} [f(x) - \mathbb{E}_{x \sim \mathcal{P}_z} [f(x)]]}{\sqrt{r_f(z, z') - 2 \log \gamma - 16 \sqrt{\frac{2d \log(8d/\delta)}{m_z \wedge m_{z'}}} - \sqrt{\frac{2d \log(8d/\delta)}{m_z}}} \\ &\leq \frac{\sigma_f(z)}{\sqrt{r_f(z, z') - 2 \log \gamma}} + \mathcal{O} \left(\left(\frac{d \log(d/\delta)}{m_z \wedge m_{z'}} \right)^{1/4} \right). \end{aligned}$$

□

Lemma 1. *Let \mathcal{F}_{K_L} be the class of K_L -Lipschitz encoders. Then for any $f_{K_L} \in \mathcal{F}_{K_L}$, $\sigma_{f_{K_L}}(z) \leq K_L \sigma_z$.*

Proof. Using Jensen's inequality and then Lipschitzness of f ,

$$\begin{aligned} \sigma_f(z) &= \mathbb{E}_{x \sim \mathcal{P}_z} [\|f(x) - \mathbb{E}_{x \sim \mathcal{P}_z} [f(x)]\|] = \mathbb{E}_{x \sim \mathcal{P}_z} \left[\left\| \int (f(x) - f(x')) p(x'|z) dx' \right\| \right] \\ &\leq \mathbb{E}_{x \sim \mathcal{P}_z} \left[\int \|f(x) - f(x')\| p(x'|z) dx' \right] \leq K_L \cdot \mathbb{E}_{x \sim \mathcal{P}_z} \left[\int \|x - x'\| p(x'|z) dx' \right] \\ &= K_L \cdot \mathbb{E}_{x, x' \sim \mathcal{P}_z} [\|x - x'\|] = K_L \delta_z. \end{aligned}$$

□

Lemma 2. *For any $g \in \mathcal{G}$, suppose there exists a $K_g > 0$ such that g is “reverse Lipschitz”, satisfying $\|f_{AE}(x) - f_{AE}(x')\| \leq K_g \|g(f_{AE}(x)) - g(f_{AE}(x'))\|$, and there exists finite b such that the reconstruction loss satisfies $\max_x \|g(f_{AE}(x)) - x\|^2 \leq b$.*

Then with probability at least $1 - \delta$,

$$\sigma_{f_{AE}}(z) \leq \frac{2K_g}{p(z|y)} \left(\hat{L}_{AE}(\mathcal{D}_y) + 2\mathfrak{R}_{n_y}^2(\mathcal{G} \circ \mathcal{F}_{AE}, id_{\mathcal{X}}) + b \sqrt{\frac{\log(1/\delta)}{2n_y}} \right)^{1/2} + K_g \sigma_z,$$

where $id_{\mathcal{X}}$ is the identity function on \mathcal{X} , and $p(z|y) = \frac{p(z)}{p(y)}$ is the probability that x drawn from $p(\cdot|y)$ has label z .

Proof. We can decompose $\sigma_{f_{AE}}(z)$ into the following using the assumption on the decoder g :

$$\begin{aligned} \sigma_{f_{AE}}(z) &= \mathbb{E}_{x \sim \mathcal{P}_z} [\|f_{AE}(x) - \mathbb{E}_{x' \sim \mathcal{P}_z} [f_{AE}(x')] \|] \leq \mathbb{E}_{x \sim \mathcal{P}_z} \left[\int \|f_{AE}(x) - f_{AE}(x')\| p(x'|z) dx' \right] \\ &\leq \mathbb{E}_{x \sim \mathcal{P}_z} \left[\int K_g \cdot \|g(f_{AE}(x)) - g(f_{AE}(x'))\| p(x'|z) dx' \right] \\ &\leq \mathbb{E}_{x \sim \mathcal{P}_z} \left[\int K_g (\|g(f_{AE}(x)) - x\| + \|x - x'\| + \|x' - g(f_{AE}(x'))\|) p(x'|z) dx' \right] \\ &= 2K_g \mathbb{E}_{x \sim \mathcal{P}_z} [\|g(f_{AE}(x)) - x\|] + K_g \mathbb{E}_{x, x' \sim \mathcal{P}_z} [\|x - x'\|]. \end{aligned} \tag{25}$$

Note that $\mathbb{E}_{x \sim \mathcal{P}_y} [\|g(f_{AE}(x)) - x\|] = \sum_{k \in S_y} \mathbb{E}_{x \sim \mathcal{P}_k} [\|g(f_{AE}(x)) - x\|] p(k|y) \geq \mathbb{E}_{x \sim \mathcal{P}_z} [\|g(f_{AE}(x)) - x\|] \times p(z|y)$, so (25) becomes

$$\begin{aligned} \sigma_{f_{AE}}(z) &\leq \frac{2K_g}{p(z|y)} \mathbb{E}_{x \sim \mathcal{P}_y} [\|g(f_{AE}(x)) - x\|] + K_g \mathbb{E}_{x, x' \sim \mathcal{P}_z} [\|x - x'\|] \\ &\leq \frac{2K_g}{p(z|y)} \sqrt{\mathbb{E}_{x \sim \mathcal{P}_y} [\|g(f_{AE}(x)) - x\|^2]} + K_g \mathbb{E}_{x, x' \sim \mathcal{P}_z} [\|x - x'\|] \\ &= \frac{2K_g}{p(z|y)} \sqrt{\hat{L}_{AE}(n_y) + \mathbb{E}_{x \sim \mathcal{P}_y} [\|g(f_{AE}(x)) - x\|^2] - \hat{L}_{AE}(n_y)} + K_g \sigma_z. \end{aligned} \quad (26)$$

where $\hat{L}_{AE}(\mathcal{D}_y) = \frac{1}{n_y} \sum_{x \in \mathcal{D}_y} \|g(f_{AE}(x)) - x\|^2$ is the reconstruction error on the training data \mathcal{D}_y . We bound the generalization error $\mathbb{E}_{x \sim \mathcal{P}_y} [\|g(f_{AE}(x)) - x\|^2] - \hat{L}_{AE}(\mathcal{D}_y)$ using Theorem 3.3 of Mohri et al. [32] to get that with probability at least $1 - \delta$,

$$\sigma_{f_{AE}}(z) \leq \frac{2K_g}{p(z|y)} \left(\hat{L}_{AE}(\mathcal{D}_y) + 2\mathfrak{R}_{n_y}^2(\mathcal{G} \circ \mathcal{F}_{AE}, \text{id}_{\mathcal{X}}) + b \sqrt{\frac{\log(1/\delta)}{2n_y}} \right)^{1/2} + K_g \sigma_z.$$

Finally, we compare against using a general autoencoder trained on the entire dataset of n points. This yields a bound

$$\sigma_{f_{AE}}(z) \leq \frac{2K_g}{p(z)} \left(\hat{L}_{AE}(\mathcal{D}) + 2\mathfrak{R}_n^2(\mathcal{G} \circ \mathcal{F}_{AE}, \text{id}_{\mathcal{X}}) + b \sqrt{\frac{\log(1/\delta)}{2n}} \right)^{1/2} + K_g \sigma_z,$$

where the only change in the result is that $p(z|y)$ is replaced with $p(z)$, the overall proportion of the subclass, and n_y is replaced with n . This highlights a tradeoff: $p(z|y) > p(z)$, but $n_y < n$. A class-conditional autoencoder may suffer from poorer generalization due to lower sample size, but its relative worst case performance on z in expectation is better. On the other hand, a general autoencoder is learned on more data, but its relative worst case performance on z in expectation is worse since the subclass is more rare w.r.t. the training data. \square

Lemma 3. For $a \in \mathcal{A}$ and any $x, x' \in \mathcal{X}$, suppose that $f_{aug} \in \mathcal{F}_{aug}$ satisfies $\|f_{aug}(a(x)) - f_{aug}(a(x'))\| \leq K_{aug} \|a(x) - a(x')\|$ for some K_{aug} and that $f(a(x)) = f(x)$ for $x \in \mathcal{D}$. Denote $\sigma_z^{aug} = \mathbb{E}_{x, x' \sim \mathcal{P}_z} [\|a(x) - a(x')\|]$. Then with probability at least $1 - \delta$,

$$\sigma_{f_{aug}}(z) \leq \frac{2}{p(z)} \left(2\mathfrak{R}_n^1(\mathcal{F}_{aug}, \mathcal{F}_{aug} \circ \mathcal{A}) + \sqrt{\frac{2 \log(1/\delta)}{n}} \right) + K_{aug} \sigma_z^{aug}.$$

Proof. We can decompose $\sigma_{f_{aug}}(z)$ into

$$\begin{aligned} \mathbb{E}_{x \sim \mathcal{P}_z} [\|f_{aug}(x) - \mathbb{E}_{x' \sim \mathcal{P}_z} [f_{aug}(x')] \|] &\leq \mathbb{E}_{x \sim \mathcal{P}_z} \left[\int \|f_{aug}(x) - f_{aug}(x')\| p(x'|z) dx' \right] \\ &\leq \mathbb{E}_{x \sim \mathcal{P}_z} \left[\int \left(\|f_{aug}(x) - f_{aug}(a(x))\| + \|f_{aug}(a(x)) - f_{aug}(a(x'))\| + \|f_{aug}(a(x')) - f_{aug}(x')\| \right) p(x'|z) dx' \right] \\ &\leq 2\mathbb{E}_{x \sim \mathcal{P}_z} [\|f_{aug}(x) - f_{aug}(a(x))\|] + K_{aug} \sigma_z^{aug}. \end{aligned} \quad (27)$$

We can bound $\mathbb{E}_{x \sim \mathcal{P}_z} [\|f_{aug}(x) - f_{aug}(a(x))\|] \leq \frac{1}{p(z)} \mathbb{E} [\|f_{aug}(x) - f_{aug}a(x)\|]$. We assume that the encoder is able to satisfy $f_{aug}(x) = f_{aug}(a(x))$ for all training data $x \in \mathcal{D}$, so (27) becomes

$$\sigma_{f_{aug}}(z) \leq \frac{2}{p(z)} \left(\mathbb{E}_x [\|f_{aug}(x) - f_{aug}(a(x))\|] - \frac{1}{n} \sum_{i=1}^n \|f(x_i) - f(a(x_i))\| \right) + K_{aug} \sigma_z^{aug}. \quad (28)$$

Then, using Theorem 3.3 from Mohri et al. [32], with probability at least $1 - \delta$

$$\mathbb{E} [\|f_{aug}(x) - f_{aug}(a(x))\|] - \frac{1}{n} \sum_{i=1}^n \|f_{aug}(x_i) - f_{aug}(a(x_i))\| \leq 2\mathfrak{R}_n^1(\mathcal{F}_{aug}, \mathcal{F}_{aug} \circ \mathcal{A}) + \sqrt{\frac{2 \log(1/\delta)}{n}}.$$

Therefore, (28) becomes

$$\sigma_f(z) \leq \frac{2}{p(z)} \left(2\mathfrak{R}_n^1(\mathcal{F}_{aug}, \mathcal{F}_{aug} \circ \mathcal{A}) + \sqrt{\frac{2 \log(1/\delta)}{n}} \right) + K_{aug} \sigma_z^{aug}.$$

□

D Additional Theoretical Results

This result is a simple example of a condition under which L_{spread} does not exhibit class-fixing permutation invariance.

Lemma 4. *Let $\phi : \mathbb{R}^+ \rightarrow \mathbb{R}^+$ be a monotonically increasing function. Suppose that for $x, x' \in \mathcal{X}$, all $f \in \mathcal{F}$ satisfy $\|f(x) - f(x')\| \leq \phi(\|x - x'\|)$. Then, L_{spread} is not invariant on class-fixing permutations under \mathcal{F} .*

Proof. First, note that L_{spread} in (2) has terms in the numerator of L_{sup} of the form $\|f(x) - f(x^+)\|$, where $h(x) = h(x^+)$. We show how to break permutation invariance using this quantity.

Fix two vectors in the embedding space \mathcal{S}^{d-1} , u_a and u_b . For x_1, x_2 in a given class, suppose that $f(x_1) = u_a$ and $f(x_2) = u_b$. We select a third point x_3 that is very close to x_1 , satisfying $\phi(\|x_3 - x_1\|) < \|u_a - u_b\|$ (this property must hold for some x_3 since ϕ is monotonic).

We construct a permutation π where $\pi(1) = 3, \pi(2) = 1, \pi(3) = 1$. We know that $\|u_a - u_b\| \leq \phi(\|x_1 - x_2\|)$. Suppose that the mapping f^π satisfies $\|f^\pi(x_3) - f^\pi(x_1)\| = \|u_a - u_b\|$. However, this implies that $\|u_a - u_b\| \leq \phi(\|x_3 - x_1\|)$, which is a contradiction. Therefore, no $f^\pi \in \mathcal{F}$ exists that is able to map the permutation to the same value as f does. As this holds for a single term in L_{spread} , it applies to L_{spread} overall, demonstrating that such an assumption on \mathcal{F} (which we find is true for a Lipschitz encoder, the autoencoder, and data augmentations) is able to break permutation invariance.

□

E Auxiliary Lemmas

Lemma 5. *Suppose \mathcal{F} is a family of functions mapping from \mathcal{X} to \mathbb{R}^d . Define $f(x)[j]$ as the j th element of $f(x)$ and suppose that for all j , $|f(x)[j]| \leq b$. Define the element-wise class $\mathcal{F}_j = \{f(\cdot)[j] : f \in \mathcal{F}\}$. Then, with probability at least $1 - \delta$ over n i.i.d. samples $\{x_i\}_{i=1}^n$,*

$$\left\| \mathbb{E}[f(x)] - \frac{1}{n} \sum_{i=1}^n f(x_i) \right\| \leq 2\mathfrak{R}_n(\mathcal{F}) + bd \sqrt{\frac{\log(d/\delta)}{2n}} \quad \forall f \in \mathcal{F},$$

where $\mathfrak{R}_n(\mathcal{F}) = \sum_{j=1}^d \mathfrak{R}_n(\mathcal{F}_j)$.

Proof. Using the triangle inequality,

$$\left\| \mathbb{E}[f(x)] - \frac{1}{n} \sum_{i=1}^n f(x_i) \right\| = \left(\sum_{j=1}^d \left(\mathbb{E}[f(x)[j]] - \frac{1}{n} \sum_{i=1}^n f(x_i)[j] \right)^2 \right)^{1/2} \leq \sum_{j=1}^d \left| \mathbb{E}[f(x)[j]] - \frac{1}{n} \sum_{i=1}^n f(x_i)[j] \right|.$$

Using Theorem 3.3 of Mohri et al. [32], we know that with probability at least $1 - \delta$,

$$\mathbb{E}[f(x)[j]] \leq \frac{1}{n} \sum_{i=1}^n f(x_i)[j] + 2\mathfrak{R}_n(\mathcal{F}_j) + b \sqrt{\frac{2 \log(1/\delta)}{n}}.$$

Applying a union bound, we have that with probability at least $1 - \delta$,

$$\left\| \mathbb{E} [f(x)] - \frac{1}{n} \sum_{i=1}^n f(x_i) \right\| \leq \sum_{j=1}^d \left(2\mathfrak{R}_n(\mathcal{F}_j) + b\sqrt{\frac{\log(d/\delta)}{2n}} \right) = 2\mathfrak{R}_n(\mathcal{F}) + bd\sqrt{\frac{2\log(d/\delta)}{n}}.$$

□

F Additional Experimental Details

We describe details about the datasets, model architectures, and hyperparameters.

F.1 Datasets

We first describe all the datasets in more detail:

- **CIFAR10**, **CIFAR100**, and **MNIST** are all the standard computer vision datasets.
- **CIFAR10-Coarse** consists of two superclasses: animals (dog, cat, deer, horse, frog, bird) and vehicles (car, truck, plane, boat).
- **CIFAR100-Coarse** consists of twenty superclasses. We artificially imbalance subclasses to create **CIFAR100-Coarse-U**. For each superclass, we select one subclass to keep all 500 points, select one subclass to subsample to 250 points, select one subclass to subsample to 100 points, and select the remaining two to subsample to 50 points. We use the original CIFAR100 class index to select which subclasses to subsample: the subclass with the lowest original class index keeps all 500 points, the next subclass keeps 250 points, etc.
- **TinyImageNet-Coarse** [29] consists of 67 superclasses constructed from the ImageNet class hierarchy [4]. The 67 superclasses are as follows: arachnid, armadillo, bear, bird, bug, butterfly, cat, coral, crocodile, crustacean, dinosaur, dog, echinoderms, ferret, fish, flower, frog, fruit, fungus, hog, lizard, marine mammals, marsupial, mollusk, mongoose, monotreme, person, plant, primate, rabbit, rodent, salamander, shark, sloth, snake, trilobite, turtle, ungulate, vegetable, wild cat, wild dog, accessory, aircraft, ball, boat, building, clothing, container, cooking, decor, electronics, fence, food, furniture, hat, instrument, lab equipment, other, outdoor scene, paper, sports equipment, technology, tool, toy, train, vehicle and weapon.
- **MNIST-Coarse** consists of two superclasses: <5 and ≥ 5 .
- **Waterbirds** [36] is a robustness dataset designed to evaluate the effects of spurious correlations on model performance. The waterbirds dataset is constructed by cropping out birds from photos in the Caltech-UCSD Birds dataset [43], and pasting them on backgrounds from the Places dataset [45]. It consists of two categories: water birds and land birds. The water birds are heavily correlated with water backgrounds and the land birds with land backgrounds, but 5% of the water birds are on land backgrounds, and 5% of the land birds are on water backgrounds. These form the (imbalanced) hidden strata.
- **ISIC** is a public skin cancer dataset for classifying skin lesions [9] as malignant or benign. 48% of the benign images contain a colored patch, which form the hidden strata.
- **CelebA** is an image dataset commonly used as a robustness benchmark [31, 36]. The task is blonde/not blonde classification. Only 6% of blonde faces are male, which creates a rare stratum in the blonde class.

Dataset	End Model Perf.		
	InfoNCE	L_{sup}	L_{spread}
CIFAR10	89.7	90.9	91.5
CIFAR10-Coarse	97.7	96.5	98.1
CIFAR100	68.0	67.5	69.1
CIFAR100-Coarse	76.9	77.2	78.3
CIFAR100-Coarse-U	72.1	71.6	72.4
MNIST	99.1	99.3	99.2
MNIST-Coarse	99.1	99.4	99.4
Waterbirds	77.8	73.9	77.9
ISIC	87.8	88.7	90.0

Table 6: End model performance training with L_{spread} on various datasets compared against contrastive baselines. All metrics are accuracy except for ISIC (AUROC). L_{spread} produces the best performance in 7 out of 9 cases, and matches the best performance in 1 case.

F.2 Model Architectures

We use a ViT model [12] (4 x 4 patch size, 7 multi-head attention layers with 8 attention heads and hidden MLP size of 256, final embedding size of 128) as the encoder for the transfer learning experiments and a ResNet50 for the robustness experiments. For the ViT models, we jointly optimize the contrastive loss with a cross-entropy loss head. For the ResNets, we train the contrastive loss on its own and use linear probing on the final layer.

For the autoencoder, we use the same encoder backbone as the main model, and use a ResNet18 in reverse order for the decoder. The convolutions are replaced with resize convolutions. We use the implementation in PyTorch Lightning Bolts¹ [15].

F.3 Hyperparameters

For the coarse dataset training, all models were trained for 600 epochs with an initial learning rate of 0.0003, a cosine annealing learning rate scheduler with T_{max} set to 100 and the AdamW optimizer. A dropout rate of 0.05 was used. We did not use weight decay. For each coarse dataset, we trained 5 separate models which jointly optimize a cross-entropy loss head with either a contrastive loss (InfoNCE, SupCon, SupCon + InfoNCE, SupCon + Class-conditional InfoNCE) or a reconstruction loss (mean squared error).

In the coarse-to-fine transfer experiments, we trained 5 separate models for each of the configurations reported in Table 3 using 5 random seeds (42, 32, 64, 128 and 72). All models were trained for 100 epochs with an initial learning rate of 0.001, a cosine annealing learning rate scheduler with T_{max} set to 100 and the AdamW optimizer. All transfer experiments were run using Tesla V100 machines.

All experiments were run using a batch size of 128 for both training and evaluation.

G Additional Experimental Results

We present additional experimental results on end model accuracy, transfer with cross entropy, and full ablations.

G.1 End Model Accuracy

See Table 6 for raw accuracy. We confirm that using L_{spread} instead of L_{sup} does not degrade end model performance.

¹https://github.com/PyTorchLightning/lightning-bolts/blob/master/pl_bolts/models/autoencoders/components.py

Table 7: Coarse-to-fine transfer learning performance (expanded table). Best in bold.

Method		CIFAR10	CIFAR100	CIFAR100-U	MNIST	TinyImageNet
Baselines	Cross Entropy	71.1 ± 0.2	54.2 ± 0.2	56.4 ± 0.4	98.7 ± 0.1	44.4 ± 0.1
	InfoNCE [7]	77.6 ± 0.1	60.5 ± 0.1	56.4 ± 0.3	98.4 ± 0.1	44.9 ± 0.1
	SupCon [27]	51.8 ± 1.2	56.1 ± 0.1	49.8 ± 0.3	95.4 ± 0.1	43.9 ± 0.1
	SupCon + InfoNCE [25]	77.6 ± 0.1	55.7 ± 0.1	48.0 ± 0.2	98.6 ± 0.1	46.1 ± 0.1
Ours	cAuto	71.4 ± 0.1	62.9 ± 0.1	58.7 ± 0.5	98.7 ± 0.1	47.1 ± 0.1
	SupCon + cNCE (L_{spread})	77.1 ± 0.1	58.7 ± 0.2	53.5 ± 0.4	98.5 ± 0.1	45.8 ± 0.1
	SupCon + cAuto	71.7 ± 0.1	63.8 ± 0.6	59.8 ± 0.3	98.7 ± 0.1	49.3 ± 0.1
	SupCon + cNCE + cAuto (THANOS)	79.1 ± 0.2	65.0 ± 0.2	59.7 ± 0.3	99.0 ± 0.1	49.6 ± 0.1

Table 8: Ablations on the autoencoder and data augmentation on CIFAR10 coarse-to-fine transfer.

General vs. Class-Conditional Autoencoder	
gAuto	41.4 ± 0.2
cAuto	71.4 ± 0.1
SupCon	51.8 ± 1.2
SupCon + gAuto	55.4 ± 0.4
SupCon + cAuto	71.7 ± 0.1
SupCon + cNCE	77.1 ± 0.1
SupCon + cNCE + gAuto	77.4 ± 0.1
SupCon + cNCE + cAuto (THANOS)	79.1 ± 0.2
cNCE With and Without Augmentation	
SupCon + cNCE - augmentation	41.7 ± 0.2
SupCon + cNCE	77.1 ± 0.1

G.2 Additional Transfer Results

We reproduce Table 3 and additionally report the performance of training with cross entropy loss (Table 7).

G.3 Ablations and Sensitivity Studies

In this section, we validate our specific theoretical claims on the class-conditional autoencoder, data augmentation, and the Lipschitzness of the decoder.

We use two ablations to validate our claims that the class-conditional autoencoder outperforms a generic autoencoder, and that data augmentation in the class-conditional InfoNCE loss is critical for inducing subclass clustering. Table 8 reports the results:

- Lemma 2 claims that a class-conditional autoencoder should outperform a generic autoencoder in coarse-to-fine transfer. Indeed, we find that using a generic autoencoder underperforms a class-conditional autoencoder by 30.0 points on CIFAR10 coarse-to-fine transfer. Furthermore, the generic autoencoder does not improve performance of SupCon or its variants as well; we observe average lift of 2.0 points, compared to 11.0 points for the class-conditional autoencoder.
- Lemma 3 claims that data augmentation in the class-conditional InfoNCE loss is key to break the permutation invariance. Removing data augmentation degrades performance by 35.4 points (and produces the permutation shown in Figure 1).

Finally, Figure 3 measures the Lipschitzness of an encoder trained with L_{spread} and the reverse Lipschitzness of the decoder from a class-conditional autoencoder. The encoder displays a high Lipschitzness constant (not very

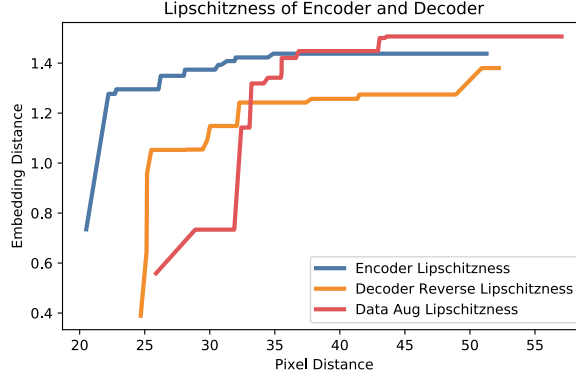


Figure 3: Measures of Lipschitzness for three ways to break permutation invariance. Encoder Lipschitzness reports pixel distance on the X axis and embedding distance on the Y axis. The Decoder reports pixel distance of the reconstruction. For augmentations, we run ten augmentations and pick the pair with the smallest ratio of pixel distance to embedding distance. The decoder is more Lipschitz than the encoder, and the encoder is more Lipschitz under augmentations than under traditional Lipschitzness.

Lipschitz). However, it displays a low Lipschitzness constant over augmentations. The decoder displays a lower reverse Lipschitzness constant. This suggests that the assumptions in Lemmas 2 and 3 are reasonable.

To measure Lipschitzness of an encoder, we measure distance in embedding space of an encoder trained with L_{spread} vs. distance in pixel space of two images (blue line). To measure reverse Lipschitzness of a decoder, we make the same measurement, but over pixel distance of decoded images from an autoencoder (orange line). To measure Lipschitzness under data augmentations, we measure the minimum ratio between embedding distance and pixel distance for 10 randomly-generated augmentations of two images (red line). The Lipschitzness constants K_L , K_g , and K_{aug} in Table 1 are the slopes of the lines tangent to each of the curves in Figure 3 from the origin.

H Synthetic Experiments

We conduct synthetic experiments to understand the optimal geometry that minimizes the asymptotic loss $L_{\text{spread}}(\boldsymbol{\mu}, \alpha)$ as defined in Section 3.2.

Setup We minimize an empirical estimate of the asymptotic loss over a set of unit vectors $\{u_i\}_{i=1}^{Kn_y}$. Denote u as a unit vector, and denote $h(u)$ as its class label. The loss we minimize is

$$(1 - \alpha) \log \frac{1}{K(K-1)n_y^2} \sum_{h(u) \neq h(u')} \exp(-\|u - u'\|^2/2\tau) + \alpha \log \frac{1}{Kn_y^2} \sum_{h(u)=h(u')} \exp(-\|u - u'\|^2/2\tau) \quad (29)$$

$$+ (1 - \alpha) \frac{1}{Kn_y^2} \sum_{h(u)=h(u')} \|u - u'\|^2/2\tau \quad (30)$$

We use `scipy.minimize` and the Sequential Least Squares Programming (SLSQP) option. We report the set of vectors that obtain the lowest loss over 5 runs with random initializations (seeds 0 – 4) as the optimal geometry.

We compute an empirical estimate of $s_f(y)$ as $\frac{1}{n_y} \sum_{u:h(u)=y} \left\| u - \frac{1}{n_y} \sum_{u':h(u')=y} u' \right\|$, and average over all classes.

Matching $\boldsymbol{\mu}$ and the optimal geometry Figure 4 displays our constructed distribution $\boldsymbol{\mu}_\theta$ as well as simulations on S^1 for $K = 2$. In particular, the right figure consists of the optimal geometry for $n_y = 20$, $\tau = 0.5$. We see that for $\alpha = 0.6$ (which is below our threshold in Theorem 2), that the optimal geometry is collapsed. For $\alpha = 0.7$, the

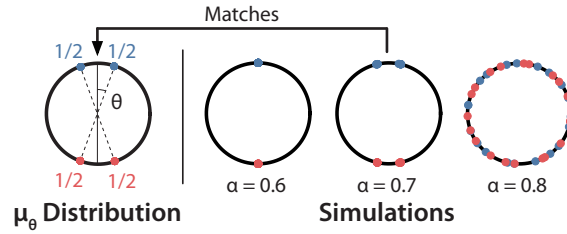


Figure 4: Left: Distribution family μ_θ . Right: Simulations of optimal geometry for binary setting on S^1 .

optimal geometry appears to closely match the parametrization of μ_θ . For $\alpha = 0.8$, which is above the theoretical threshold, the optimal geometry is uniform per class.

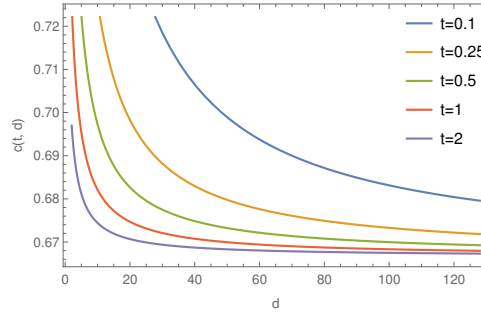


Figure 5: The value of $c(\tau, d)$, which determines the range of α for which μ_θ obtains lower loss than δ_v and σ_{d-1} .

Computing $c(\tau, d)$ Next, we compute the value of $c(\tau, d)$, the constant in Theorem 2, over values of τ and d to verify that $\alpha \in (2/3, c(\tau, d))$ is a valid range for which the optimal geometry is neither collapsed nor uniform. This quantity depends on the Wiener constant of the Gaussian $\frac{1}{2\tau}$ -energy on \mathcal{S}^{d-1} , which does not have a closed form expression (see (17)). Figure 5 shows that $c(\tau, d) > 2/3$ for d up to 128 (which is the dimension of our embedding space) and for $\tau = 0.1, 0.25, 0.5, 1, 2$.

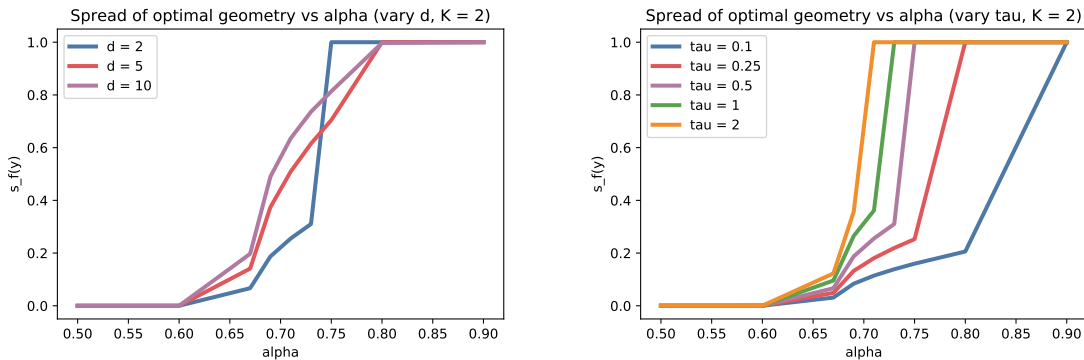


Figure 6: The spread $s_f(y)$ of the optimal geometry for a given α in the binary setting, $n_y = 8$. Left: how optimal spread changes based on dimension d of the embedding space. Right: how optimal spread changes based on the temperature hyperparameter τ .

Varying τ and d for $K = 2$ We plot α versus spread $s_f(y)$ for the optimal geometry in the binary setting, and in particular we vary τ and d in Figure 6. We compute the optimal geometries over $\alpha = 0.5, 0.6, 0.67, 0.69, 0.71, 0.73, 0.75, 0.8, 0.9$. Figure 6 left shows how the spread changes as α increases for dimensions $d = 2, 5, 10$ and $n_y = 8$ samples,

and the right shows how the spread changes as α increases for $\tau = 0.1, 0.25, 0.5, 1, 2$. Note that for all dimensions and all τ , the optimal geometry has nonzero spread starting at $\alpha = 0.67$, matching our theoretical findings. The point at which the uniform distribution becomes optimal is less clear, but we do not expect it to closely match $c(\tau, d)$, as this constant depends on the asymptotic free energy, whereas the free energy over a finite configuration (even if it converges to the uniform distribution asymptotically) is hard to compute for $n_y > d + 1$. Nevertheless, this figure matches our findings that an α that induces appropriate spread exists over a certain range, outside of which behavior is strictly collapsed or uniform.

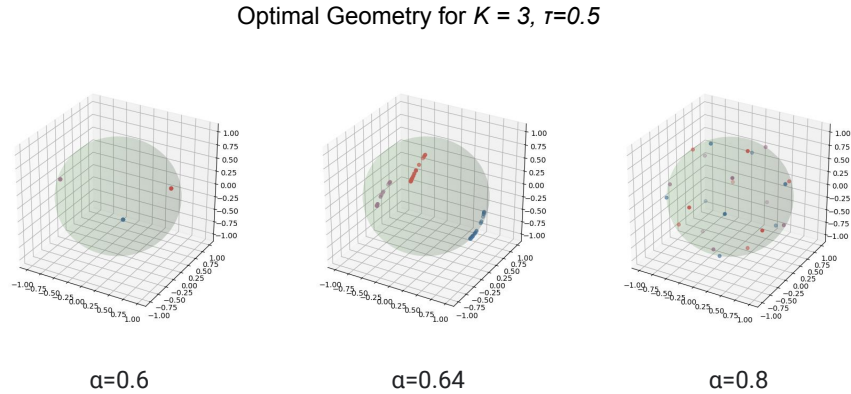


Figure 7: Visualizations of the optimal geometry for $n_y = 8, K = 3$ in \mathcal{S}^2 across various α .

Multiclass Analysis for $K = 3$ Similar to Figure 4, we show for $K = 3$ and \mathcal{S}^2 that the optimal geometry is collapsed for low α , sufficiently spread for a particular range, and uniform for high α . Figure 7 displays the optimal geometry for $n_y = 8, \tau = 0.5$ across $\alpha = 0.6, 0.64, 0.8$, suggesting that the multiclass case exhibits similar behavior as α varies.

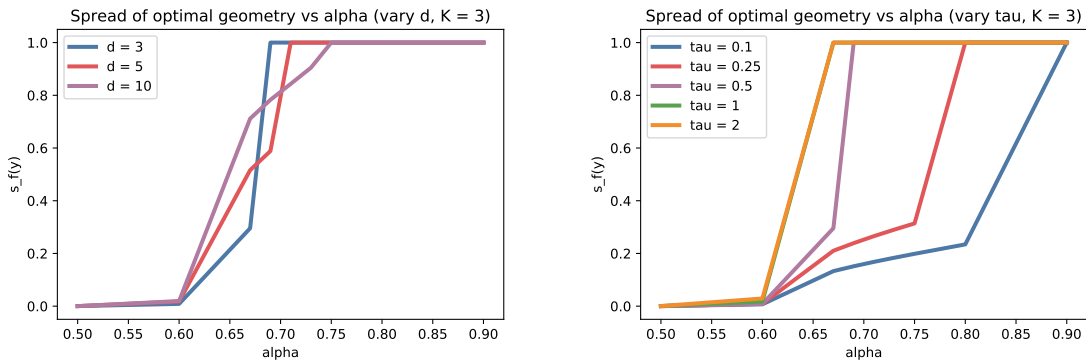


Figure 8: The spread $s_f(y)$ of the optimal geometry for a given α when $K = 3, n_y = 8$. Left: how optimal spread changes based on dimension d of the embedding space. Right: how optimal spread changes based on the temperature hyperparameter τ .

We plot α versus spread $s_f(y)$ for the optimal geometry in the multiclass setting, and again we vary τ and d in Figure 8. We see that the behavior of the optimal geometry's spread $s_f(y)$ across α is roughly similar to that of $K = 2$ in Figure 6.